Possible Eoarchean records of the geomagnetic field preserved in the Isua Supracrustal Belt, southern west Greenland

Claire I. O. Nichols[a,b], Benjamin P. Weiss[a], Athena Eyster[c], Craig R. Martin[a]. Adam C. Maloof[d], Nigel M. Kelly [e], Mike J. Zawaski [f,g], Stephen J. Mojzsis [f,h,i,j], E. Bruce Watson [k], Daniele J. Cherniak[l]

[a]Department of Earth, Atmospheric and Planetary Sciences, Massachusetts Institute of Technology, 77 Massachusetts Avenue, Cambridge, MA 02139, USA
[b]Department of Earth Sciences, University of Oxford, South Parks Road, Oxford, OX1 3AN, UK
[c]Department of Geoscience, University of Wisconsin-Madison, 1215 West Dayton Street, Madison, WI 53706, USA
[d]Department of Geosciences, Princeton University, Guyot Hall, Princeton, NJ 08544, USA
[e]Bruker Nano Analytics, 5465 E. Cheryl Parkway, Madison, Wisconsin 53711, USA
[f]Department of Geological Sciences, University of Colorado Boulder, UCB 399, Boulder, CO 80309, USA
[g]Department of Geology and Geophysics, Texas A&M University, 108 Halbouty Building, 3115 TAMU, College Station, Texas 77843-3115, USA
[h]Origins Research Institute, Research Centre for Astronomy and Earth Sciences, MTA Centre of Excellence, 15-17 Konkoly Thege Miklos ut Budapest, 1121 Hungary
[i]Department of Lithospheric Research, University of Vienna UZA 2, Josef-Holaubek-Platz 2 A-1090 Vienna, Austria
[j]Institute for Earth Sciences, Friedrich-Schiller University Burgweg 11 07749 Jena, Germany
[k]Department of Earth and Environmental Sciences, Rensselaer Polytechnic Institute, 110 Eighth Street, Troy, NY 12180, USA
[l]Ion Beam Laboratory, State University of New York at Albany, 1400 Washington Avenue Albany, NY 12222, USA

Key Points:

- The northernmost part of the northeast Isua Supracrustal Belt experienced one significant metamorphic event 3.69 Ga.
- Banded iron formations hold stable magnetization that passes several paleomagnetic field tests indicating preservation of an Eoarchean geomagnetic field.
- Paleomagnetic results suggest the Eoarchean geomagnetic field was similar in strength to today and may have been reversing.

Corresponding author: Claire I. O. Nichols, `claire.nichols@earth.ox.ac.uk`

Abstract

We present paleomagnetic field tests that hint that a record of Earth's 3.7-billion-year (Ga) old magnetic field may be preserved as a chemical remanent magnetization acquired during amphibolite-grade metamorphism in the banded iron formation from the northeastern Isua Supracrustal Belt. Multiple petrological and geochronological lines of evidence indicate that the northern most part of Isua has not experienced metamorphic temperatures exceeding 350°C since the Eoarchean, suggesting the rocks have not been significantly heated since magnetization was acquired. We use a 'pseudo' baked contact test to assess paleodirections in the banded iron formation that pre-date the intrusion of the 3.26-3.5 Ga Ameralik dyke swarm. We demonstrate that specimens that pass this test also go on to pass a fold test and may also pass a reversal test. We recover what appears to be the oldest known whole rock record of the geomagnetic field, and oldest known records of reversals suggesting that Earth's magnetic field behaviour in the Eoarchean may have been similar to that observed today.

Plain Language Summary

Recovering ancient records of Earth's magnetic field is highly challenging because the magnetization in rocks is often reset by heating during tectonic burial over their long and complex geological histories. We have shown that rocks from the Isua Supracrustal Belt in West Greenland are exceptionally well preserved and have not been substantially heated or deformed since 3.7-billion-years-ago. We have used multiple lines of evidence to demonstrate this, including paleomagnetic field tests which allow magnetic overprints to be identified, the metamorphic mineral assemblages across the area, and the temperatures at which radiometric ages of the observed mineral populations are reset. We show that Earth's magnetic field was broadly similar in strength to today, and discuss the implications of this for habitability and early dynamo generation.

1 Introduction

Recovering a record of the geodynamo throughout Earth history is key to understanding the role of magnetic fields in habitability, the thermal evolution of the early Earth, and the power sources required to sustain planetary dynamos for billions of years. The preservation of a temperate climate and liquid water on Earth's surface has been attributed to the presence of a magnetosphere that shielded the atmosphere from erosion by the solar wind (Tarduno et al., 2014). However, recent atmospheric escape models suggest that the presence of a planetary dynamo can enhance escape (Lundin et al., 2007; Gunell et al., 2018; Gronoff et al., 2020). Therefore accurate observations of the intensity of Earth's magnetic field during periods of atmospheric loss will be key for determining the role of a magnetosphere in preserving habitable environments.

The geodynamo currently is driven by compositional convection as the inner core solidifies. However, the age of the inner core remains contentious, with estimates of its initial nucleation ranging from 4.2–0.5 Ga ago (Biggin et al., 2015; Bono et al., 2019; Konôpková et al., 2016; Ohta et al., 2016; Pozzo et al., 2012; Zhang et al., 2020). If the core has a low thermal conductivity (< 100 W m^{-1} K^{-1}), the inner core is predicted to be old (> 1 Ga) and compositional convection could have been sustained throughout much of Earth's history. If the thermal conductivity is high ($100 - 250$ W m^{-1} K^{-1}) and the inner core is young, heat loss would be predominantly via conduction (which would preclude a core dynamo) or else the core underwent compositional convection and sustained a dynamo via precipation of light elements such as Mg and Si at the core-mantle boundary (O'Rourke & Stevenson, 2016; Badro et al., 2016; Hirose et al., 2016). Alternatively, an early core dynamo might have been driven mechanically (e.g., by tides) or else was generated in a basal magma ocean (Blanc et al., 2020; Landeau et al., 2022). In order to resolve this conundrum, a robust paleomagnetic record that constrains both the strength and stability of the magnetic field before, during and after inner core solidification is required to distinguish between proposed dynamo models.

The aim of this study is to extend the ancient whole-rock paleomagnetic record beyond 3.5 Ga. The previous oldest whole-rock paleomagnetic studies were conducted on rocks from the 3.5 Ga Barberton Greenstone Belt in South Africa and the Duffer Formation, Australia (Tarduno et al., 2010; Biggin et al., 2011; Herrero-Bervera et al., 2016). A paleointensity of 6.4 μT was recovered from the Duffer Formation (Herrero-Bervera et al., 2016), although it remains unresolved whether this represents a genuinely weak geomagnetic field record, or inefficient magnetic remanence acquisition. Paleomagnetic studies on single zircon crystals have argued for evidence of an active geodynamo during the Archean and Hadean with a similar field strength to today (Tarduno et al., 2015, 2020). However, other studies have demonstrated that the magnetic carriers in these zircons are secondary in origin and the magnetization is likely an overprint that post-dates the formation of the zircons by billions of years (Tang et al., 2019; Weiss et al., 2015, 2018; Borlina et al., 2020; Taylor et al., 2023). An additional limitation of these single-crystal paleomagnetic studies is that no directional information is preserved (the zircons are detrital). If the mechanism of remanence acquisition is determined in whole-rock samples, then the age of magnetization can be verified using paleomagnetic field tests, allowing the stability and intensity of the geomagnetic field to be reliably investigated.

Here, we begin the effort to extend the whole-rock paleomagnetic record to 3.7 Ga ago by recovering natural remanent magnetizations (NRMs) from banded iron formations (BIFs) in the Isua Supracrustal Belt (ISB), southern west Greenland. BIFs have not typically been targeted for paleomagnetic study, and previous results have been hampered by issues with thermal alteration (Schmidt & Clark, 1994; Wabo et al., 2018). The Isua BIF has an unusually simple mineralogy, comprised of alternating bands of quartz and magnetite with minor amphibole at the boundary between the two phases. The northernmost part of the northeast ISB (north of $65°11'$N) is exceptionally well preserved, with localized regions of low-strain where pillow structures and original sedimentary features are still observable (Nutman & Friend, 2009). We outline several lines of evidence below that suggest this part of the belt only experienced on significant metamorphic event ca. 3.69 Ga.

The paleomagnetic results presented in this study primarily focus on the remanence acquired by magnetite in BIFs. The origin of magnetite in BIFs has been highly debated, although it is now commonly accepted that magnetite is not a primary phase formed directly via precipitation from the water column. The majority of magnetite in BIFs is now considered to be the product of metamorphism and diagenesis of precursor ferro-ferric oxides and hydroxides (Rasmussen & Muhling, 2018; Konhauser et al., 2017; Nutman et al., 2017). The magnetite in the Isua BIF formed during an Eoarchean metamorphic event (Dymek & Klein, 1988; Frei et al., 1999). This age is supported by direct Pb-Pb dating of the magnetite in the Isua BIF, returning an age of 3.691 $\pm$ 0.022 Ga (Frei et al., 1999; Frei & Polat, 2007). There is therefore significant uncertainty surrounding the mechanism by which the magnetite in the BIF acquired its paleomagnetic remanence. The magnetite may have grown via direct crystallization, acquiring a grain-growth CRM by growth through a blocking volume (Kobayashi, 1959; Stokking & Tauxe, 1987, 1990). Alternatively, magnetite may have replaced existing phases in the BIF, acquiring a phase-transformation CRM. The nature of this type of CRM is poorly understood, and in this case is further hampered by the ongoing debate regarding the primary mineralogy in BIFs which could include green rust, ferrihydrite and greenalite (Halevy et al., 2017; Johnson et al., 2018; Nutman et al., 2017; Tosca et al., 2016). There is also likely to be a thermal component to the acquired CRM given the high metamorphic and hydrothermal temperatures (450 – 550°C) the magnetite cooled from (Dymek & Klein, 1988; Frei et al., 1999).

We consider both magnetite Pb-Pb ages and paleomagnetic field tests to verify the age of magnetization. Three previous studies have investigated the potential of Pb-Pb dating for magnetite (Frei et al., 1999; Frei & Polat, 2007; Erel et al., 1997). These studies were carried out on the Isua BIF, and the Brockman Iron Formation from the Hamersley basin, western Australia. They were motivated by the absence of detrital minerals that are typically used for U-Pb geochronology, such as zircon, apatite and baddeleyite in BIFs (the apatite observed in the Isua BIF is considered to be associated with early hydrothermal events ca. 3.63 Ga; Frei et al. (1999)). Magnetite contains low but measurable concentrations of U (0.2–0.4 ppm) and Pb (0.2–0.7 ppm) with radiogenic Pb representing $\sim 2\%$ of total Pb (Gelcich et al., 2005). The low amount of U and radiogenic Pb makes it challenging to directly recover a U-Pb isochron from magnetite. However, stepwise leaching allowed both uranogenic and thorogenic arrays to be successfully recovered and a Pb-Pb isochron to be calculated.

BIF specimens used to recover the Pb-Pb ages reported by Frei et al. (1999) and Frei and Polat (2007) were collected at 65.20818°N, 49.75855°W (purple star in Figure 1), near sites 8A/A, B, C and D in this study. The studies recovered Pb-Pb isochron ages of 3.691 ± 0.049 Ga and 3.691 ± 0.022 Ga and suggest magnetite formed during Eoarchean amphibolite-grade metamorphism. The Pb-Pb age of the magnetite has not been perturbed or reset since this early metamorphic event. However, previous studies were unable to interpret these ages in terms of the subsequent thermal history of the area, since the Pb diffusion rate in magnetite was unconstrained. Recent Pb diffusion measurements and closure temperature estimates for magnetite (E. B. Watson et al., 2023) allow us to determine that the Pb-Pb age was acquired during a metamorphic event exceeding 120–400°C, consistent with the 450–550°C peak metamorphic temperature of the Eoarchean event recovered from the grunerite-bearing, pyroxene and minnesotaite-absent mineral assemblage in the BIF (Dymek & Klein, 1988). In addition, our results suggest that the BIF has not been heated to temperatures exceeding 350°C in the subsequent Neoarchean and Proterozoic metamorphic events.

The closure temperature of the U-Pb system for magnetite (E. B. Watson et al., 2023) has significant applications for paleomagnetic studies. For thermal remanences, the difference between the closure temperature and the magnetic blocking temperature will allow the relationship between the magnetite age and the timing of NRM acquisition to be determined. In addition, for metamorphic rocks where the age of magnetite relative to the age of the bulk rock is often uncertain this technique permits the age of the magnetite, and therefore the oldest possible time of CRM acquisition, to be dated directly.

We conclude that the northernmost region of the northeast ISB has not experienced temperatures above 350°C since 3.69 Ga. We show that regardless of the mechanism of remanence acquisition, the age of magnetization can be verified by the Pb-Pb age of magnetite, since any subsequent low-temperature (150–400°C) thermal events will partially or fully reset the U-Pb age. We argue that the magnetite in Isua carries a chemical remanent magnetization (CRM) formed during a complex series of metamorphic and metasomatic events ca. 3.7 Ga (Frei et al., 1999; Dymek & Klein, 1988; Nutman et al., 2022), and this remanence has not been overprinted by subsequent metamorphic events (Figure 2). For specimens that pass paleomagnetic field tests and exhibit stable demagnetization, pseudo-Thellier experiments yielded a paleointensity estimate of > 15 μT for the Eoarchean geomagnetic field.

1.1 Geologic Setting

The northeastern part of the ISB is subdivided into three main terranes separated by faults (Figure 1). The 3.7 Ga northern terrane, the focus of this study, is sandwiched between a northwest terrane and the 3.8 Ga southwest terrane (Nutman & Friend, 2009).

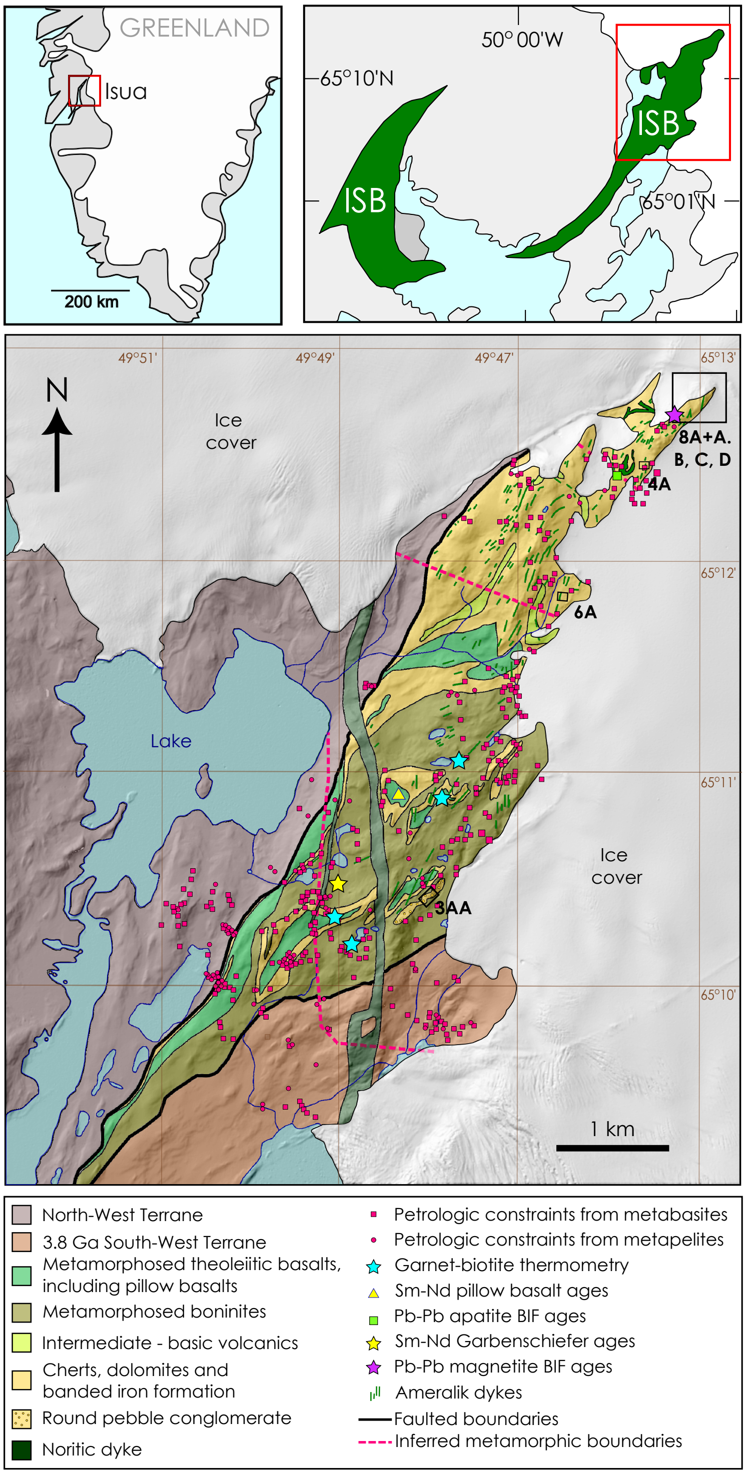

Figure 1. A simplified geological map (after Nutman and Friend (2009)) depicts the north-eastern part of the ISB. The two smaller maps show the entire extent of the ISB and its location in Greenland. Previous tectonothermal constraints on the metamorphic history of the ISB are shown by the coloured symbols: petrological constraints from metabasites (pink squares) and metapelites (pink circles) and the inferred metamorphic boundaries (pink dashed lines; Arai et al. (2015); Komiya et al. (2002)); garnet-biotite thermometry (blue stars; Rollinson (2002, 2003)); Sm-Nd pillow basalt ages (yellow triangle; Polat et al. (2003)); Pb-Pb apatite ages (green square; Nishizawa et al. (2005)); Sm-Nd plagioclase amphibole ages (yellow star; Gruau et al. (1996)); and Pb-Pb magnetite BIF ages (purple star; Frei et al. (1999); Frei and Polat (2007)). The sites where paleomagnetic field tests were conducted as part of this study are labelled 3AA, 4A, 6A, 8A/A, B, C and D.

The southern part of the northern terrane is dominated by metamorphosed boninites, interspersed with dolomites, conglomerates, and basalts. Further north in the field area, magnetite-bearing cherts begin to dominate, and the northernmost extent of the area is almost exclusively made up of BIF. These 3.7 Ga sediments and volcanics were intruded by dykes that are assumed to be part of the Ameralik dyke swarm, which was emplaced 3.26–3.5 Ga ago (ages constrained by U-Pb zircon dating) across much of the Nuuk district of southwest Greenland (Nutman et al., 2004; Nutman & Friend, 2009). The final major intrusive event in the area was the emplacement of a large ($>$ 100 m wide) noritic dyke, which trends north-south across the northeast part of the ISB cross-cutting all the major lithologies (Nutman & Friend, 2009). Zircons from the dyke have a U-Pb age of 2.214 ± 0.010 Ga (Nutman et al., 1995).

The northern terrane has experienced three metamorphic events during the Eoarchean, Neoarchean and Proterozoic, evidence for which are summarised in Table 1. The Eoarchean metamorphic event was amphibolite grade resulting in the formation of a single generation of garnets (Rollinson, 2003) and the growth of grunerite and magnetite in the BIF at 3.69 Ga (Dymek & Klein, 1988; Frei et al., 1999). Garnet-biotite thermometry indicates a peak temperature of 470–550°C (Rollinson, 2002). This metamorphic event was likely the result of the collision between the 3.7 Ga northern terrane and the 3.8 Ga southern terrane at 3.69–3.66 Ga based on zircon U-Pb ages (Nutman & Friend, 2009).

A Neoarchean tectonothermal event associated with the juxtaposition of the Isukasia and Kapisilik terranes occurred ca. 2.85 Ga (Nutman, Bennett, Friend, Yi, & Lee, 2015; Frei et al., 1999; Gruau et al., 1996; Polat et al., 2003). The metamorphic grade increases from north to south towards the mylonitized region between the two terranes, which lies $>$ 20 km south of the ISB. The southernmost part of the ISB experienced temperatures of 500–600°C (Gruau et al., 1996), with peak metamorphic temperatures in the northernmost region substantially below 400°C, since no perturbation in BIF apatite or magnetite Pb-Pb ages is observed for this time period (Nishizawa et al., 2005; Frei et al., 1999). The Ameralik dykes were metamorphosed in this event and in the northernmost part of the area the mineral assemblage was transformed from olivine, pyroxenes and plagioclase to a combination of actinolite, chlorite, epidote, albite, quartz, sphene, serpentine and magnetite, indicating lower greenschist grade metamorphism (360–400°C; Komiya et al. (2004); Arai et al. (2015)).

A subsequent thermal perturbation in the area at 1.5–1.6 Ga is not observed in most of the metamorphic assemblages across the area, and most notably the 2.2 Ga norite dyke retains it's primary igneous mineralogy (Nutman et al., 2022). The only evidence for this later event is in a perturbation in the Pb-Pb apatite age in the BIF, and the resetting of the Rb-Sr age in the pillow basalts (Nishizawa et al., 2005; Polat et al., 2003). Since neither system has undergone complete homogenization and resetting, this event is interpreted to have been a low temperature ($\sim$ 320°C) overprint and not sufficient to produce new mineral growths or reaction rims on the existing metamorphic mineral assemblages.

1.2 Sample lithologies

In the southern part of the northeast ISB are outcrops of what has been described as a round pebble conglomerate (Site 3AA). This conglomerate is sedimentary in origin (Fedo, 2000), with sedimentary beds defined by variations in the matrix grain size. The conglomerate is made up of rounded clasts that vary from 0.5–30 cm in diameter. Pebble clasts have been rotated into the cleavage plane and stretched parallel to this foliation. The clasts have a range of lithologies including amphibolite, quartzite, iron formation, felsic volcanic and sandstone comprised of mafic grains. The conglomerate also contains quartz veins that are boudinaged and comprise crystalline quartz, whereas the quartzite clasts still preserve remanents of individual quartz grains, and variations in grain-

Table 1. A summary of the evidence for each of the three metamorphic events experienced by the northeast Isua Supracrustal Belt.

Eoarchean Metamorphic Event (ca. 3.69 Ga)	
The BIF was metamorphosed to an assemblage containing grunerite, cummingtonite, actinolite and magnetite indicating amphibolite grade metamorphism.	Dymek and Klein (1988)
Magnetite in the BIF in the northern ISB has a Pb-Pb age of 3.69 Ga.	Frei et al. (1999); Frei and Polat (2007)
Garnet grew during a single metamorphic event, at temperatures between 470–550°C based on garnet-biotite geothermometry.	Rollinson (2003, 2002)
Neoarchean Metamorphic Event (ca. 2.85 Ga)	
Sm-Nd ages in pillow basalt rims reset to 2.567 Ga in southern part of the northeast ISB.	Polat et al. (2003).
No perturbation of Pb-Pb apatite ages in the banded iron formation suggests peak metamorphic temperature substantially below 400°C in northern part of ISB.	Nishizawa et al. (2005).
Ameralik dykes (emplaced 3.26–3.5 Ga) retain primary igneous textures and are only weakly metamorphosed to a greenschist grade assemblage in northern part of ISB, so must post-date amphibolite grade event.	Nutman, Bennett, and Friend (2015); Arai et al. (2015)
Pb-Pb magnetite ages in BIF in the southwestern part of the ISB are 2.84 ± 0.05 Ga.	Frei et al. (1999)
Sm-Nd plagioclase and amphibole ages from the Garbenschiefer unit in the southern part of the ISB are 2.849 ± 0.116 Ga, indicating a metamorphic temperature of 500–600°C.	Gruau et al. (1996)
Proterozoic Metamorphic Event (ca. 1.5–1.6 Ga)	
Perturbation of Pb-Pb apatite age ca. 1.5 Ga in the BIF suggests an event below 400°C.	Nishizawa et al. (2005)
The Pb-Pb age of magnetite in the BIF was nor perturbed by this event, suggesting its thermal influence in the northernmost part of the northeast ISB was minimal.	Frei et al. (1999)
Perturbation of Sm-Nd age and resetting of the Rb-Sr errorchron in pillow basalt rims at 1.604 Ga indicates a metamorphic temperature of $\sim$ 320°C.	Polat et al. (2003)
2.2 Ga noritic dyke retains its primary igneous mineralogy, indicating no substantial metamorphism after this time, only hydrothermal alteration.	Nutman et al. (2022)

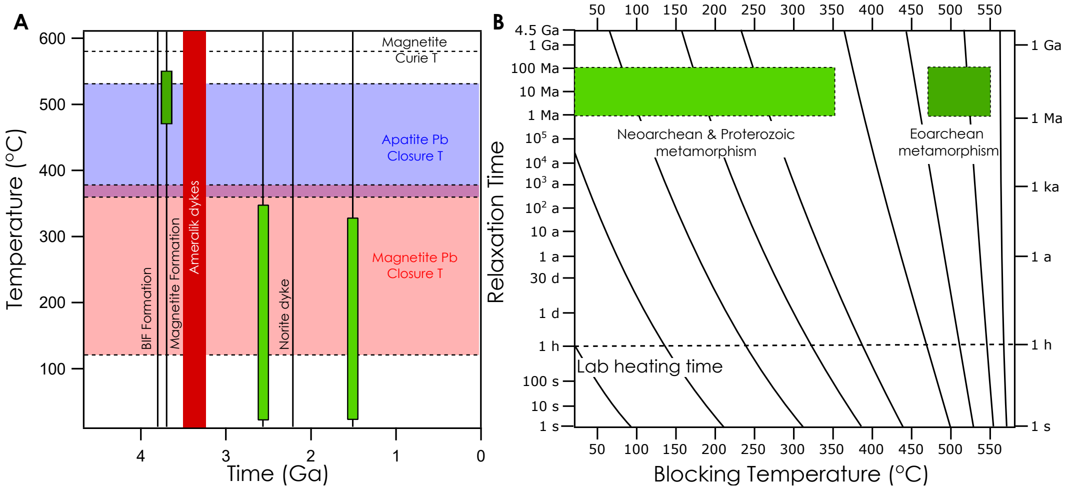

Figure 2. The thermal history of the ISB. **A** Temperature versus time plot showing the thermal events that have influenced the ISB. The green rectangles represent the three metamorphic events in the Eoarchean (dark green), Neoarchean and Proterozoic (pale green). The timing of BIF formation, magnetite formation, the metamorphic events and dyke emplacement events are shown by vertical lines. Since both the Pb-Pb age of the magnetite and the apatite still preserve an age of 3.7–3.8 Ga we use the closure temperatures of these systems (shown by the red and blue regions, respectively) to show the upper limit on the temperature experienced by the BIF since magnetite formation during Eoarchean metamorphism. The magnetite Curie temperature, above which remanence is entirely reset is also shown. **B** A Pullaiah diagram (Pullaiah et al., 1975) shows that remanence acquired in any of the metamorphic events can be unblocked in the lab during heating times of 1 hour up to temperatures $<$ 580°C. The diagram also indicates that the Neoarchean and Proterozoic events cannot entirely overprint the magnetization acquired during Eoarchean metamorphism even during events lasting of order 100 Ma, although they may result in thermal overprints $<$ 450°C.

size within each clast. The variety in the composition, dimensions and morphology of the clasts was used to argue against a purely tectonic origin for the conglomerate (Fedo et al., 2001; Nutman et al., 1984). The conglomerate was metamorphosed to amphibolite grade with peak temperatures of 500–600°C during both the Eoarchean and Neoarchean tectonothermal events (Table 1).

BIF forms in the northernmost part of field area (Figure 1). It varies from a magnetite-bearing chert to a typical BIF with alternating layers of magnetite and quartz with a varying degree of amphibole and carbonate. The BIF has been split into various categories depending on its mineral assemblage (Aoki et al., 2016; Dymek & Klein, 1988). Here, we define BIF as the quartz-magnetite formation defined by Dymek and Klein (1988) and the gray-type BIF defined by Aoki et al. (2016). The BIF has a Rb-Sr age of 3.7 $\pm$ 0.14 Ga (Moorbath et al., 1973) and apatite from the BIF yields a Pb-Pb age of 3.9 $\pm$ 0.2 Ga (Nishizawa et al., 2005). Two generations of magnetite are observed in the BIF, both of which were formed after primary deposition of Fe-clays such as greenalite (Nutman et al., 2017). The first generation of magnetite replaced the primary mineralogy in the original depositional bands yields a Pb-Pb age of 3.69 $\pm$ 0.22 Ga (Frei et al., 1999). A subsequent hydrothermal event at 3.63 $\pm$ 0.07 Ga introduced secondary veins of magnetite into the BIF as well as pyrite and apatite (Frei et al., 1999; Nishizawa et al., 2005).

The BIF in the northeast region of the ISB is intruded by part of the Ameralik dyke swarm (Nutman & Friend, 2009), which was emplaced 3.26–3.5 Ga ago across much of the Nuuk district of southwest Greenland (Nutman et al., 2004). We assume that the dykes intruding the BIF are all part of the Ameralik dyke swarm, and refer to them all as Ameralik dykes although previously in the literature some have been referred to as Tarssartôq dykes (White et al., 2000; Nutman et al., 2004; Nutman, 1986). These dykes are mafic in composition and variably deformed and boudinaged, and primary intrusive contacts with the country rock often are sheared (Nutman et al., 2004). The Ameralik dykes were emplaced after the Eoarchean metamorphic events which generated the magnetite in the primary depositional banding in the BIF (Frei et al., 1999; Dymek & Klein, 1988), but prior to subsequent Neoarchean and Proterozoic metamorphic events.

2 Materials and Methods

2.1 Paleomagnetic sampling and field tests

We conducted two field campaigns to the ISB between 29th July – 6th August 2018 and 16th July – 27th July 2019. We carried out geological mapping and collected oriented drill core and block samples of a conglomerate and six sites where mafic Ameralik dykes intrude the BIF. A total of three-hundred-and-eight specimens were used for subsequent paleomagnetic analysis (Table 2).

Sampling was carried out using a water-cooled Pomeroy EZ Core Drill to extract 2.5-cm-diameter cores. Cores were oriented using a Pomeroy Orienting Fixture and both magnetic and sun compass readings were taken. We primarily relied upon sun compass readings, since the BIF generated strong localized magnetic fields which disturbed magnetic compass readings. Cores were extracted using brass chisels to avoid remagnetizing the specimens.

Conglomerate tests, pseudo-baked contact tests, fold tests and reversal tests were all conducted at various sites (Table 2) within the field area (Buchan, 2007; Graham, 1949). For the conglomerate test, individual clasts were drilled, as well as the surrounding matrix. For the pseudo-baked contact tests, both the middle and edge of the dykes were drilled, although chilled margins were not obviously visible. The surrounding country rock was drilled at regular intervals of 0.3–1 m, preferentially targeting regions of rock that were absent of fractures, deformation or veining. Specimens were acquired up to $>$ 3 radii from the dyke to ensure sufficient sampling in the unbaked regions. Each area

Table 2. A summary of the sites where paleomagnetic field tests were carried out. The first column is the site name, the second and third are the latitude and longitude of the site, respectively, the fourth is the number of specimens used for paleomagnetic analyses, the fifth is the type of paleomagnetic field test that was carried out.

Site	Location		No. of specimens measured	Paleomagnetic Field Test
	Latitude (° N)	Longitude (° W)		
3AA	65.1744	49.8000	28	Conglomerate test - round pebble conglomerate
4A	65.2073	49.7589	32	Baked contact test - BIF and Ameralik dyke
6A	65.1982	49.7740	25	Baked contact test - BIF and Ameralik dyke (boudinaged)
8A and A	65.2095	49.7579	46	Baked contact test - BIF and Ameralik dyke
B	65.2111	49.7528	54	Baked contact test - BIF and Ameralik dyke
C	65.2106	49.7528	32	Baked contact test - BIF and Ameralik dyke
D	65.2115	49.7533	46	Baked contact test - BIF and Ameralik dyke

was explored in detail to ensure no other dykes existed close to the unbaked region which may have influenced the recovered paleomagnetic signals. Watson's V_W statistic was used to determine if a distinct direction was acquired close to and far away from each dyke. Both fold and reversal tests were carried out on unbaked BIF directions that passed Watson's V_W test (Tauxe et al., 1991).

2.2 Paleomagnetic analyses

Drill cores were cut into 1-cm thick discs using the ASC Scientific dual-blade rock saw at MIT. BIF samples were further cut down to 1-mm thick slices using the Buehler IsoMet® low speed saw in the MIT Paleomagnetism Laboratory due to their exceptionally strong magnetic moments. Other lithologies (conglomerate clasts, matrix and Ameralik dykes) were measured as 1-cm thick discs. Specimens were demagnetized using the 2G Enterprises superconducting quantum interference device (SQUID) rock magnetometer, housed in a magnetically-shielded room made of mu-metal with a background DC field of < 200 nT in the MIT Paleomagnetism Laboratory.

Specimens were demagnetized sequentially using several techniques; a subset of specimens were initially placed in liquid nitrogen to remove the majority of the multidomain component (Halgedahl & Jarrard, 1995). In all cases where a liquid nitrogen step was carried out, a sister specimen was also demagnetized without this step in order to ensure this didn't introduce any bias into the recovered data. All specimens were then AF demagnetized in steps of 2 mT from 2–10 mT along three orthogonal axes to 'clean' the specimens of low-coercivity, unstable multidomain components. Specimens were then thermally demagnetized between 100–580°C in gradually decreasing temperature steps ranging from 50–5°C. Samples were heated for 1 hour to ensure any magnetization acquired during metamorphic events lasting between 1000 years and 1 Ma was unblocked (Pullaiah et al., 1975).

Stable components of magnetization were identified using principal component analysis (Kirschvink, 1980). Stable, origin-trending components were defined as those where the maximum angular deviation (MAD) is greater than the deviation angle (dAng). Component directions were plotted in geographic coordinates in Stereonet (Allmendinger et al., 2013; Cardozo & Allmendinger, 2013) and Fisher statistics calculated to constrain the mean and α_{95} for each related group of specimens. Where the degree of scatter was large a Watson test for randomness was also conducted (G. S. Watson, 1965).

A suite of sister specimens were AF demagnetized along three orthogonal axes from 0–145 mT in steps of 5 mT, with a small subset demagnetized up to 400 mT in steps of 100 mT between 200–400 mT to identify high-coercivity components. Three specimens (A05c, A07c, C02b) were used for pseudo-Thellier experiments. A 50 μT ARM (50 μT bias DC field applied under a 260 mT alternating field) and 40 mT IRM were imparted to each specimen and then AF demagnetized up to 145 mT. Demagnetization of the ARM was compared to demagnetization of the NRM to calculate paleointensities, B_{anc}, using the following calibration:

$$B_{anc} = \frac{\Delta NRM}{\Delta ARM}\frac{B_{lab}}{a} \tag{1}$$

where $a = 3.28$ is the calibration factor for magnetite (Paterson et al., 2016). For some specimens, the NRM demagnetization had directional components in opposing directions, resulting in substantial curvature in the demagnetization plots. To remove this curvature, vector subtraction was used to isolate the moment magnitude in order to calculate $\frac{\Delta NRM}{\Delta ARM}$. The ARM demagnetization was also compared to the IRM demagnetization to verify the paleointensity recording fidelity of the BIF specimens. The recovered paleointensity, B_{rec}, was estimated using the following:

$$B_{rec} = \frac{\Delta ARM}{\Delta IRM} f \tag{2}$$

where $f = 3000$ (Gattacceca & Rochette, 2004).

The recovered paleointensities were combined to find a weighted average and uncertainty using the following equations:

$$\bar{\mu} = \frac{\sum_{n=1}^{i} w_i \mu_i}{\sum_{n=1}^{i} w_i} \tag{3}$$

where $\bar{\mu}$ is the weighted mean, $w_i = \frac{1}{\sigma_i^2}$ where σ_i is the standard deviation recovered for each individual paleointensity measurement and μ_i is each recovered paleointensity value. The weighted uncertainty is then calculated using:

$$\bar{\sigma} = \sqrt{\left(\frac{\sum_{n=1}^{i} w_i \left(\mu_i - \bar{\mu}\right)^2}{\frac{n-1}{n}\sum_{n=1}^{i} w_i}\right)} \tag{4}$$

where n is the number of specimens.

2.3 Rock magnetic analyses

First-order reversal curve (FORC) diagrams, hysteresis loops and backfield curves were measured using a Lakeshore Princeton Measurements Corporation (PMC) MicroMag 2900 Series alternating gradient magnetometer (AGM) at the University of Cambridge. Five BIF specimens (4A11, 6A09, 6A15, 8A06 and 8A19) were measured. FORCs were measured with a saturating field H_{sat} of 1 T in field steps of 2 mT. A total of 263 curves were measured with an averaging time of 300 ms. FORC diagrams were processed using the software package FORCinel (Harrison & Feinberg, 2008). Hysteresis loops were measured up to saturating fields of 0.5–1 T in order to calculate the hysteresis parameters M_{rs}, M_s and H_c which are the saturation remanent magnetization, saturation magnetization and coercivity, respectively. H_{cr}, the coercivity of remanence, was calculated from the backfield curve when the magnetization is zero. Backfield curves were measured up to a saturating field of 1 T. Backfield curves were also used to estimate the coercivity spectra of each population of magnetite grains within each specimen using MAX UnMix (Maxbauer et al., 2016).

3 Results

3.1 Paleomagnetic carriers

The NRMs of three lithologies were subjected to thermal demagnetization: conglomeratic clasts (of varying mineralogy, with most being quartz-rich), dolerite dykes (part of the Ameralik dyke swarm) and BIF. Thermal demagnetization shows that for the conglomerate clasts and dolerite, the majority of magnetization is removed between 300–400°C (Figures S14 and S15). In the BIF samples, a sharp drop in magnetization close to 580°C suggests the magnetic carrier is magnetite (Figure 6 and S16–18). None of these carriers represent the primary mineralogy and therefore magnetization is interpreted as a TCRM imparted during amphibolite grade metamorphism (450–550 °C). Alternating-field (AF) demagnetization removed NRM with an intensity $<$ 0.1 times that for isothermal remanent magnetization (IRM), indicating that specimens have not been lightning remagnetized (Figure 11).

The domain state of magnetite in the BIF was characterized by comparing AF and thermal demagnetization, backfield curves and a Lowrie test (Lowrie & Fuller, 1971). The Lowrie test (Figure 3) showed that AF demagnetization of the NRM was significantly more stable than demagnetization of a 40 mT IRM, indicating that the NRM is primarily carried by stable, single-domain magnetite grains. All specimens plot in the multidomain (MD) region of the Day plot and the FORC diagrams also revealed predominantly MD behaviour (Figure 4). Multidomain magnetite was efficiently demagnetized at low field strengths of $<$ 10 mT (Hodych, 1982). Both high temperature (HT; $>$ 400°C) and high-coercivity (HC; $>$ 60 mT) directions are similar (Figure S13) although HT directions are slightly influenced by low-coercivity, multidomain overprints which are not effectively removed during thermal demagnetization. Backfield curve acquisition revealed three populations of magnetite grains (Figure 4); the largest population (64–100 % of grains) is dominated by grains with a mean coercivity of $\sim$ 10–20 mT, suggesting they are multidomain. A second population (15–27 % of grains) has a mean coercivity ranging from $\sim$ 60–70 mT and a third population ($<$ 10 % of grains) has a mean coercivity of $>$ 150 mT. These higher coercivity grains are likely stable single domain or single vortex magnetite grains (Hodych, 1982).

3.2 Conglomerate test

A conglomerate test (Site 3AA) was carried out (Figures 1 and S14) in the southern part of the area, that experienced amphibolite grade metamorphism in both the Eoarchean and Neoarchean metamorphic events (Table 1). Twenty-five clasts and three matrix specimens were demagnetized up to 585°C (Table S5). The vast majority of specimens exhibited unstable demagnetization behaviour shown by high maximum angular deviation (MAD) values $>>$ 10. Ten clasts and one matrix specimen exhibited at least two clear stable components, at least one of which had a MAD ¡ 10. Eight clasts exhibited a stable high temperature (HT; up to 350°C) component. A test for randomness was carried out on recovered HT directions from these eight clasts. The length of the eight resultant vectors $R = 6.35$ exceeds $R_o = 5.26$, demonstrating that the hypothesis of randomness can be rejected with $p = 0.01$ significance (G. S. Watson (1965); Table S2). Twelve low temperature (LT) components from nine clast specimens gave a resultant vector $R = 7.69$ which exceeds $R_o = 6.55$, indicating that the hypothesis of randomness can be rejected. The LT and HT directions defined by the clasts are also similar (281/83, $\alpha_{95} = 25$ and 300/61, $\alpha_{95} = 31$, respectively) suggesting both the HT and LT components have

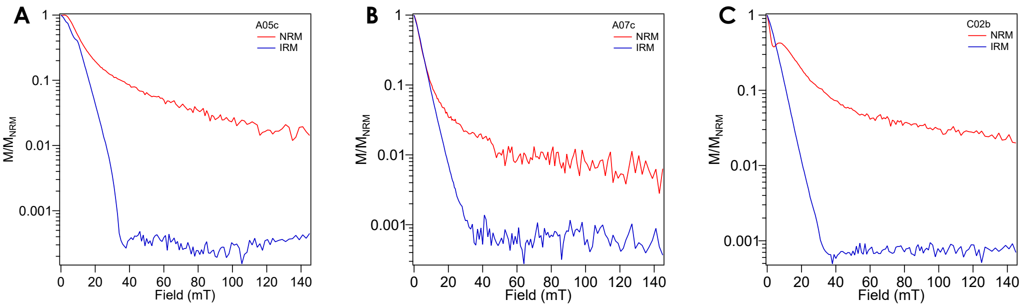

Figure 3. Results of a Lowrie test conducted to determine whether the NRM in BIF specimens is carried by MD or SD grains. The NRM (red curves) and IRM (blue curves) were demagnetized up to 145 mT. For all three specimens shown, **A** A05c, **B** A07c and **C** C02b, the NRM is signficantly more stable than the IRM, indicating that the NRM is predominantly carried by single-domain magnetite.

experienced the same overprint (Figure S14). None of the samples showed a stable component that extended significantly beyond 350°C. The conglomerate test therefore fails and demonstrates that the conglomerate has been remagnetized in later metamorphic events following its original deposition, most likely during both the Eoarchean and Neoarchean metamorphic events, both of which reached amphibolite grade in the southern part of the area.

3.3 Baked contact tests

We carried out pseudo-baked contact tests (where NRM component directions are compared for BIF that was thermally perturbed by the intrusion and BIF sufficiently far from the intrusion to be unaffected, and the intrusion direction itself is not considered) at six sites in the northernmost part of the eastern ISB (Figure 1). We were unable to carry out traditional baked contact tests, since the magnetization in the Ameralik dykes post-dates their emplacement, and was acquired during greenschist-grade metamorphism during the Neoarchean tectonothermal event (Table 1).

We targeted areas where Ameralik dykes had intruded through the BIF, and therefore represent a distinct, localized thermal perturbation that should only have influenced the BIF immediately adjacent to the dykes. We found that in all cases, the dyke NRM component directions were poorly defined and scattered, with low peak blocking temperatures (< 350°C) at each site and between sites (Figure S15) suggesting variable CRM acquisition during Neoarchean metamorphism (Komiya et al., 2004) or remanence dominated by multidomain carriers.

We infer the boundary between BIF that was baked and BIF that remained largely unbaked by the dyke intrusion by using a simple thermal diffusion model for a basaltic dyke intruding into silicate country rock (Jaeger, 1964) and by also considering the distance at which HT components of the NRM begin to converge on a single direction (Figure 5). The radii of the dykes at Sites 4A, 6A, 8A, A, B, C and D were 3 m, 3 m, 5 m, 6.5 m, 3.35 m, 3.35 m and 8.5 m, respectively. The width of the baked region is influenced by a number of factors including the temperature of dyke emplacement, the subsequent cooling-rate of the dyke and the fluid flux into the surrounding BIF which determines the degree of conductive versus convective heat transport. Given that all the dykes are doleritic in composition (White et al., 2000; Nutman & Friend, 2009; Komiya et al., 2004) it is plausible to assume they had similar emplacement temperatures. Dis-

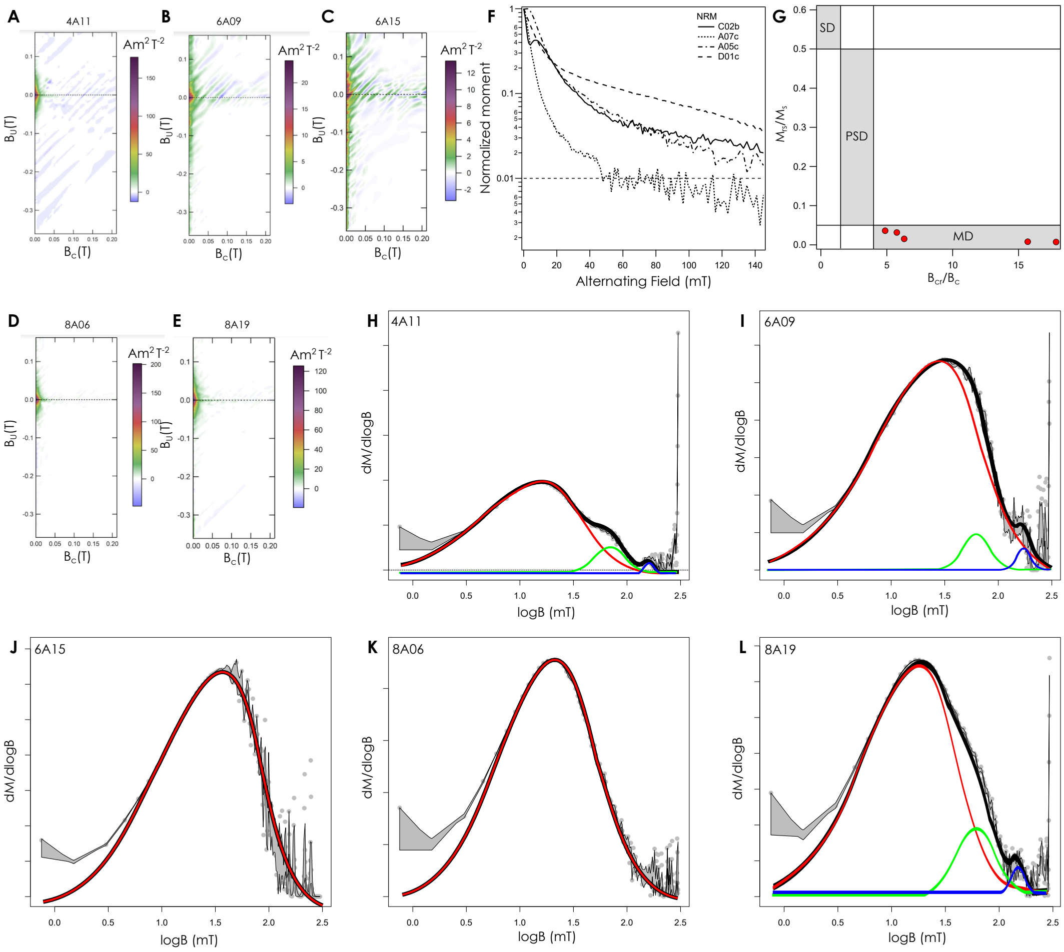

Figure 4. Rock magnetic analyses on banded iron formation specimens. **A**,**B**,**C**,**D** and **E** show FORC diagrams for specimens 4A11, 6A09, 6A15 and 6A19, respectively. In all cases, the FORC diagrams exhibit typical MD behaviour. However, **F** shows that during AF demagnetization, remanence is removed up to fields exceeding 145 mT suggesting stable SV or SD grains are present. **G** A Day plot summarizing the hysteresis behaviour of the samples. **H**–**L** show coercivity distributions derived from backfield curves. Three populations of magnetite grains are shown by the red Gaussian curves and the blue and green Gaussian curves, which represent MD and SD/SV populations of magnetite grains, respectively.

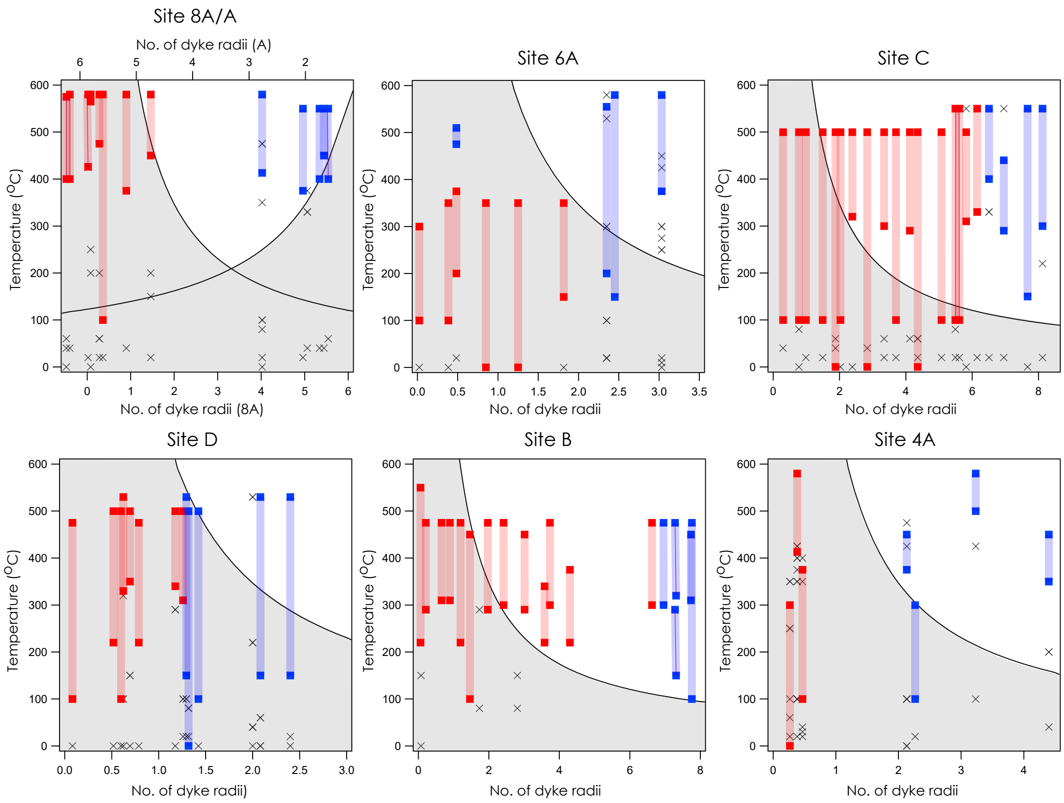

Figure 5. Thermal profiles calculated using the model reported by Jaeger (1964) show the temperature to which the country rock has been thermally perturbed (grey region) as a function of dyke radius. All recovered components of magnetization at each site are shown as black crosses. The components used to calculate the baked directions are shown by the red bars and the components used to calculated the unbaked directions are shown by the blue bars.

crepancies between the convergence of unbaked directions and the thermal diffusion model may reflect varying conditions in fluid flow and subtle variations in lithology (e.g., as seen for site 6A).

The paleomagnetism of the Ameralik dykes

The Ameralik dykes are highly variable in terms of their paleomagnetic stability and the recovered paleodirections. The dykes at site A and 6A show the most stable behaviour, and it is notable that the stable component is demagnetized by $\sim 350°$C, consistent with magnetization acquired during Neoarchean lower greenschist metamorphism. The dykes no longer contain any of their primary igneous mineralogy and magnetite is formed during the replacement of olivine (Komiya et al., 2004), and it has been noted that the magnetite content varies widely among the dykes most likely reflecting different degrees of equilibration during metamorphism, as well as varying abundances of olivine initially. The inconsistency in paleomagnetic stability between Ameralik dykes can therefore be explained by acquisition of a relatively low temperature (350°C) CRM, as well as variations in the abundance, size and shape of magnetite present.

At site 6A, four specimens of the Ameralik dyke were demagnetized up to 580°C. Three of the dyke samples (6A01, 6A02 and 6A03) are demagnetized by 350°C, and define a single direction of 321°/29° ($\alpha_{95} = 13°$). The fourth dyke sample (6A04) which comes from near the edge of the intrusion was entirely demagnetized at $< 100°$C.

At site 4A, eight Ameralik dyke specimens (including four sister specimens) were demagnetized up to 580°C. The majority of magnetization was removed from the Ameralik dyke specimens by 350°C, and specimens generally show unstable magnetization behaviour (for example, a consistent component cannot be recovered even from sister specimens). Four specimens (4A01-2, 4A02-1, 4A02-2 and 4A04-2) showed a stable component between 100–350°C which defined a direction 204/-73 ($\alpha_{95} = 25$).

At site 8A/A two Ameralik dykes, A and 8A, intrude close to one another (37.5 m apart) through a well exposed section of BIF. The two dykes define distinct directions and have contrasting magnetic properties. Eight specimens (including four sister specimens) of dyke A define a direction of 253°/-25° ($\alpha_{95} = 4°$). The magnetization is very stable until $\sim 330°$C and the majority ($> 90\%$) of magnetization is removed between 325–375°C. Six specimens of dyke 8A were demagnetized, five of which had resolvable components and two of which had stable components at temperature exceeding 300°C. The two specimens with stable HT components (8A01 and 8A03B) show broadly similar behaviour to dyke A, although the behaviour is generally less stable with considerably higher MADs ($\sim 20°$ for the HT components of dyke 8A, compared to $< 5°$ for all specimens of dyke A). The two HT components from dyke 8A define the direction 120°/-53° ($\alpha_{95} = 39°$).

At site B, twelve Ameralik dyke specimens were measured. Nine of the dyke specimens were thermally demagnetized and three were AF demagnetized. The dyke specimens exhibited unstable demagnetization behaviour often with a MAD $> 20°$. The majority of magnetization was removed below 300°C for thermally demagnetized specimens, and below 60 mT for AF demagnetized specimens. LT ($< 150°$C) components were highly scattered. However, seven specimens exhibited a stable component up to a maximum temperature of 220–425°C which define a consistent direction of 045/69 ($\alpha_{95} = 18$). This is consistent with the direction 340°/66° ($\alpha_{95} = 32°$) recovered from the three AF demagnetized specimens.

At site C eight dyke specimens (including four sister specimens) were thermally demagnetized. Six of the dyke specimens exhibited highly unstable thermal demagnetizations and no stable components of magnetization could be resolved. Two sister specimens (C24a and C24b) exhibited stable demagnetization up to 550°C (MAD $< 10°$).

At site D, six dyke specimens (including two sister specimens) were thermally demagnetized. HT ($> 300°C$) components were recovered from three of the dyke specimens defining the direction 246°/42° ($\alpha_{95} = 51°$). A distinct LT direction ($< 300°C$) was also recovered for all four specimens (including averages of sister specimens) defining the direction 135°/53° ($\alpha_{95} = 28°$).

Pseudo-baked contact tests

For each pseudo-baked contact test, Watson's V_W statistic was calculated (G. S. Watson, 1983); this statistic determines whether the HT baked and unbaked directions are statistically distinct representing a passed pseudo-baked contact test, or indistinguishable representing a failed test.

At site 8A/A, fifteen BIF specimens were measured (including one sister specimen; Table 3). BIF specimens < 7.3 m from the contact with dyke 8A (> 30 m from dyke A) exhibited LT ($\leq 200°C$), MT ($\leq 450°C$) and HT ($> 500°C$) components with generally stable demagnetization behaviour (MAD $< 10°$). A significant portion of the magnetization is lost by 100°C and most of the remaining magnetization is lost by 400°C (Figure 6). Seven baked BIF specimens had a HT component that defined the direction 187°/-24° ($\alpha_{95} = 59°$). Unbaked BIF specimens > 20 m from dyke 8A and > 10 m from dyke A generally exhibited a stable MT ($\leq 450°C$) and HT ($> 500°C$) component. The HT components define a direction of 025°/62° ($\alpha_{95} = 47°$). The calculated Watson V_W statistic for the unbaked and baked BIF directions exceeds the critical V_W value, indicating a passed pseudo-baked contact test with 95% confidence (Figure 7A).

At site 6A (Figure 6), the baked (< 5.45 m from the contact) BIF specimens contained an MT component which is demagnetized $< 400°C$. Five baked specimens defined a coherent direction of 249°/56° ($\alpha_{95} = 28°$). One BIF specimen, 6A10, collected 1.45 m from the dyke had a HT component ($T > 475°C$, Table 3) that was consistent with the direction recovered from three unbaked BIF specimens (6A15, 6A16 and 6A17) collected > 5.45 m from the dyke contact, suggesting its original HT magnetization was not overprinted during dyke emplacement. The four specimens demagnetize up to $> 500°C$ and define the direction of 048°/46° ($\alpha_{95} = 25°$). Watson's V_W value for the unbaked and baked directions exceeds the critical value of V_W, indicating a passed pseudo-baked contact test with 95% confidence (Figure 7B).

At site C, twenty one BIF specimens were both thermally and AF demagnetized (Figure 6). Baked BIF specimens taken < 20 m from the dyke contact defined a consistent HT (stable up to 500°C) direction of 174°/71° ($\alpha_{95} = 21°$). Eleven sister specimens of BIF were also AF demagnetized. Seven of these specimens lie within 20 m of the dyke contact and define a HC direction of 208°/70° ($\alpha_{95} = 26°$). When combined, the HC and HT direction is 169°/79° ($\alpha_{95} = 22°$). Further than 20 m from the dyke a distinct direction emerges for both thermally and AF demagnetized BIF samples with a direction of 313°/30° ($\alpha_{95} = 26°$) and 276°/53° ($\alpha_{95} = 35°$), respectively. When combined, these give a HC and HT direction of 294°/25° ($\alpha_{95} = 18°$). Watson's V_W statistic for the combined HC and HT directions exceeds the critical value of V_W, indicating a passed pseudo-baked contact test with 95% confidence (Figure 7C).

At site D, seventeen BIF specimens (including 3 sister specimens) were thermally demagnetized (Figure S18, Table 4). BIF specimens taken < 11 m from the dyke contact defined scattered directions at low temperatures ($< 290°C$), and define a HT ($> 310°C$) direction of 229°/17° ($\alpha_{95} = 79°$). BIF samples taken from ≥ 11 m from the dyke contact define a HT ($\geq 500°C$) component defining the direction 303°/48° ($\alpha_{95} = 43°$). Using Watson's V_W statistic, we found that the two directions are statistically distinct at the 95% confidence interval (Figure 7D). However, site D is not included in further analysis, since the uncertainty in the recovered directions is large and overlaps, and

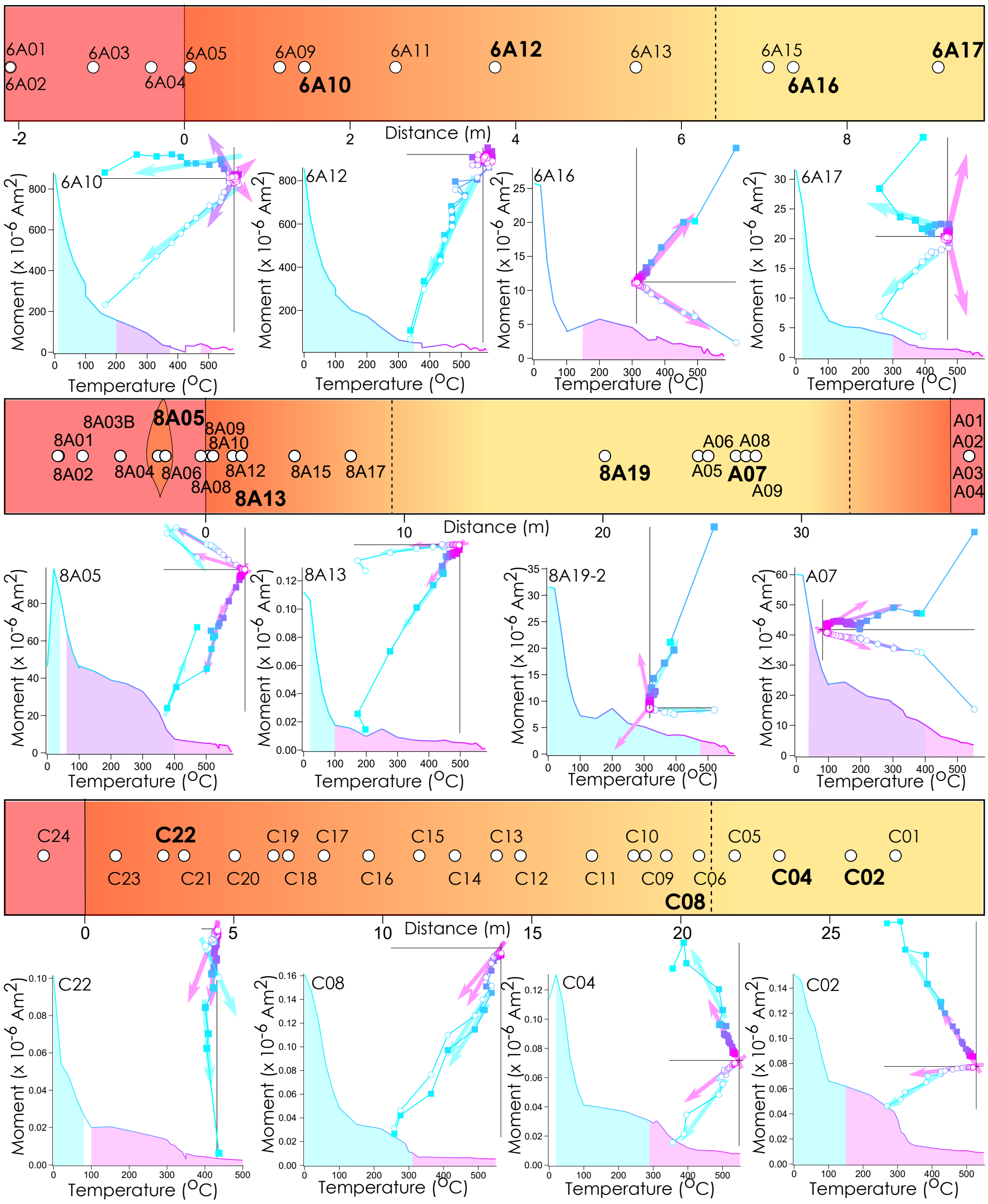

Figure 6. Passed pseudo-baked contact tests for sites 6A (top panel), 8A/A (middle panel) and C (lower panel). The schematic diagrams show the distance of each sample (white circle) from the Ameralik dyke (red) and the location of the baked (orange) and unbaked (yellow) regions. Representative thermal demagnetization curves and zijderveld diagrams are shown for a range of distances from the intrusion-BIF contact. Zijderveld diagrams are show using 'E, Horizontal' and 'N, Up' as the x, y projection and inclination and declination are shown by open circles and closed squares, respectively. LT, MT and HT components are shown in blue, purple and pink, respectively.

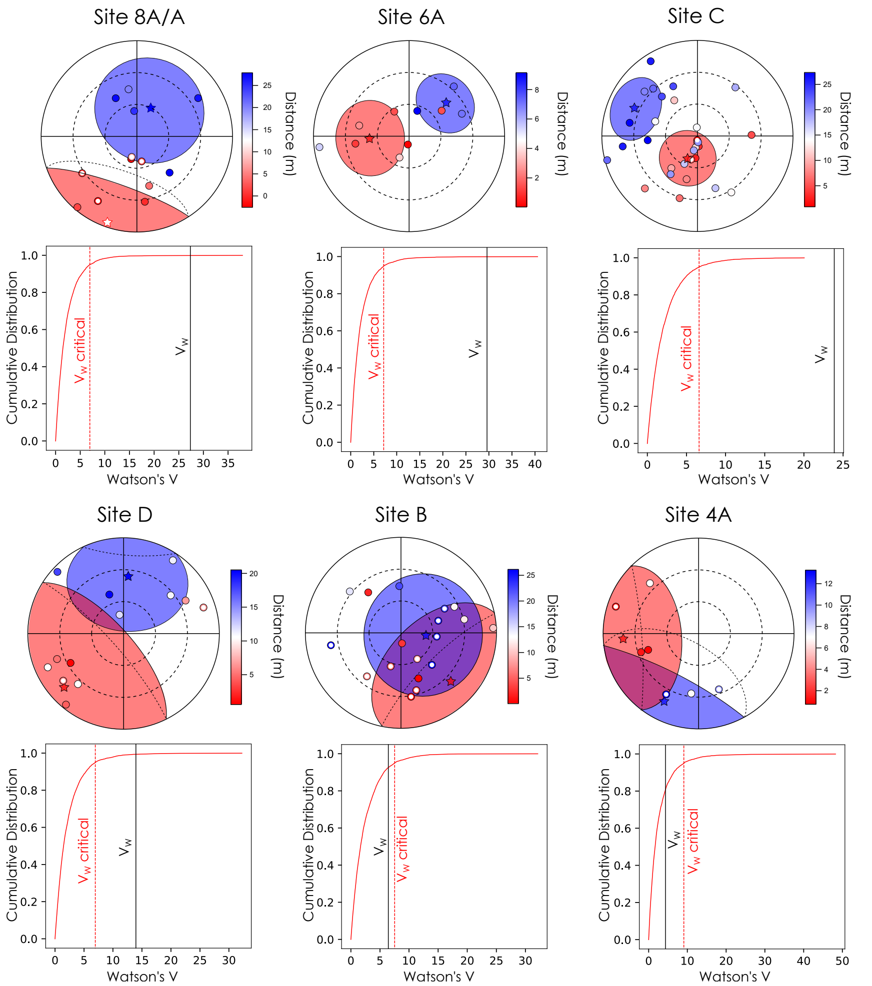

Figure 7. Bootstrapping tests to determine whether baked (red) and unbaked (blue) BIF directions are distinct to 95% confidence by calculating Watson's V_W statistic. If V_W calculated from the measured paleodirections is greater than the critical value of V_W calculated from bootstrapped data with the same number of samples and degree of clustering, κ, the our pseudo-baked contact test is considered to pass. For **A**, **B** and **C**, which show data for sites 8A/A, 6A and C, respectively, V_W is greater than the critical value indicating passed pseudo-baked contact tests. For **D**, the pseudo-baked contact test technically passes, although we do not include in further analysis because of the high degree of scatter in the directions and the fact sampling did not extend sufficiently far from the baked zone (Figure 5). **E** and **F** show data for sites B and 4A, respectively, V_W is less than the critical value indicating failed pseudo-baked contact tests.

Table 3. A summary of the directions used in the passed pseudo-baked contact tests at sites 8A/A, 6A and C.

Sample	Distance from dyke 1 (m)	Distance from dyke 2 (m)	AF/thermal?	Range (mT or °C)	Dec (°)	Inc (°)	Origin trending?	MAD	dAng
Site 6A baked									
6A05	0.07		thermal	100–300	188	82	×	1	1
6A09	1.15		thermal	100–350	262	39	×	17	22
6A10	1.45		thermal	200–375	329	63	×	11	15
6A11	2.55		thermal	0–350	282	42	✓	14	5
6A12	3.75		thermal	0–350	204	68	✓	5	1
6A13	5.45		thermal	150–350	263	5	✓	21	19
Site 6A unbaked									
6A15	7.05		thermal	200–555	67	36	✓	13	12
6A16	7.35		thermal	150–580	42	27	✓	8	7
6A17	9.1		thermal	375–580	18	65	✓	25	23
6A10	1.45		thermal	475–510	52	51	✓	19	17
Site 8A/A baked									
8A05	-2.4	39.9	thermal	400–575	211	-19	✓	9	2
8A06	-2.0	39.5	thermal	400–580	194	68	✓	11	1
8A09	0.1	37.4	thermal	426–580	173	28	✓	7	2
8A10	0.4	37.1	thermal	565–580	236	-28	×	14	37
8A12	1.4	36.1	thermal	475–580	169	-66	✓	7	5
8A13	1.8	35.7	thermal	100–580	220	3	✓	11	4
8A15	4.5	33.0	thermal	375–580	166	42	✓	4	1
8A17	7.3	30.2	thermal	450–580	194	-70	✓	5	4
Site 8A/A unbaked									
8A19	20.1	17.4	thermal	413–580	350	45	✓	9	2
A05	24.8	13.3	thermal	375–550	354	66	✓	14	5
A07	26.7	11.4	thermal	400–550	58	22	✓	14	10
A08	27.2	10.9	thermal	450–550	331	49	✓	19	0
A09	27.7	10.4	thermal	400–550	138	44	✓	16	1
Site C baked									
C23a	1		thermal	100–500	183	-86	✓	17	2
C22b	2.6		thermal	100–500	185	69	✓	4	1
C21a	3.3		thermal	100–500	173	80	✓	11	4
C20a	5		thermal	100–500	89	39	✓	15	10
C19a	6.3		thermal	0–500	195	-67	✓	17	2
C18b	6.8		thermal	100–500	196	29	✓	9	1
C18a	6.8		AF	25–145	182	84	✓	3	3
C17b	8		thermal	320–500	194	48	✓	11	6
C17a	8		AF	25–145	225	20	×	9	24
C16a	9.5		thermal	0–500	219	51	✓	4	3
C15a	11.2		thermal	300–500	327	50	×	8	13
C14b	12.4		thermal	100–500	189	79	✓	6	2
C13a	13.8		thermal	290–500	149	28	✓	15	9
C12a	14.6		thermal	0–500	356	82	×	7	10
C12b	14.6		AF	30–145	289	48	✓	25	4
C11a	17		thermal	100–500	161	38	✓	8	4
C11b	17		AF	55–145	205	61	×	12	15
C10a	18.4		thermal	100–550	38	32	✓	10	4
C09a	18.8		thermal	100–550	194	76	✓	5	3
C08a	19.5		thermal	310–500	215	46	✓	20	14
C08b	19.5		AF	10–145	174	84	×	2	4
C06a	20.6		thermal	330–550	310	25	✓	7	2
Site C unbaked									
C05a	21.8		thermal	400–550	317	29	✓	23	11
C05b	21.8		AF	10–145	255	2	×	2	5
C04a	23.3		thermal	290–440	334	38	✓	5	3
C04b	23.3		AF	10–145	318	40	×	2	3
C02a	25.7		thermal	150–550	328	7	×	3	3
C02b	25.7		AF	10–145	262	19	×	1	5
C01a	27.2		thermal	300–550	265	43	✓	4	3
C01b	27.2		AF	10–145	281	25	×	13	19

thermal diffusion modelling suggests sampling did not extend far enough from the intrusion (Figure 5).

At site B, twenty-one BIF specimens were thermally demagnetized (Figure S17, Table 4). BIF specimens experienced alteration during heating to temperatures exceeding 475°C and it is therefore unclear how far above this temperature these stable components extend. Specimens which exhibited a MAD $< 10°$ and a stable component up to 475°C were assessed for the pseudo-baked contact test. At a distance of > 23 m from the dyke contact, six unbaked BIF specimens define a consistent direction of 302°/69° ($\alpha_{95} = 44°$). Baked BIF specimens < 23 m from the dyke contact define two broadly antipodal directions. Of the sixteen specimens in this region, seven have a negative inclination and define the direction 186°/-43° ($\alpha_{95} = 23°$). The recovered directions for the baked and unbaked BIF are indistinguishable to 95% confidence using Watson's V_w statistic (Figure 7E).

At Site 4A, eleven BIF specimens (including four sister specimens) were demagnetized up to 580°C (Figure S16, Table 4). The BIF specimens showed stable demagnetization, although the recovered directions are highly scattered, even when compared to sister specimens. 4A12 and 4A13, which were collected furthest from the contact at 9.7 and 13.2 m respectively, had MT and HT components which defined the direction 179°/-49° ($\alpha_{95} = 34°$) suggesting that the BIF has been entirely overprinted, or is unable to retain a stable magnetization direction. This is consistent with the large drop in magnetization during a preliminary liquid nitrogen step, suggesting the vast majority of magnetite in the specimens is multidomain. The BIF specimens defined a coherent LT direction up to temperatures of 350°C with direction 235°/46° ($\alpha_{95} = 28°$) consistent with an overprint acquired during Neoarchean metamorphism. The LT and HT components in the BIFs overlap with the HT component in the dyke, again suggesting a pervasive overprint on this field site. The recovered directions for the baked and unbaked BIF are indistinguishable to 95% confidence using Watson's V_w statistic (Figure 7F).

3.4 Fold Test

We carried out a fold test on unbaked and baked BIF from the three sites that passed the pseudo-baked contact test: 6A, 8A/A and C. Each set of unbaked directions were untilted based on the basal bedding measurement (parallel to the banding in the BIF) for each site (Figure 8). Planar bedding measurements were 108°/60° (site C), 145°/67° (site 8A/A) and 346°/83° (site 6A). Each set of measurements were tilted progressive from -10% to 100% tilt correction by changing the dip of the correction and holding the strike constant. For each degree of tilting, a mean direction was calculated for all three data sets combined, and the primary eigenvalue, τ_1 was calculated for the mean direction. The larger the value of τ_1 the greater the degree of clustering of directions, regardless of their polarity (Tauxe & Watson, 1994).

For the baked directions, the maximum value of τ_1 was recovered between -5–45% untilting (Figure 9). This suggests that the directions in the baked BIF were acquired post-tilting due to the juxtaposition of the 3.7 Ga northern terrane and 3.8 Ga southern terrane at 3.69 Ga (Nutman & Friend, 2009), most likely during the emplacement of the Ameralik dyke swarm 3.26–3.5 Ga (Nutman et al., 2004). It is unknown whether the original magnetization in the dykes was uniform in orientation, but at 20% tilting a southern magnetization direction is recovered from the baked BIF (Figure 9).

For the unbaked BIF directions the maximum value of τ_1 was recovered between 80–110% untilting, suggesting a passed fold test (Figure 9). This indicates that the magnetization in the unbaked BIF was acquired pre- or syn-tilting during Eoarchean metamorphism and the juxtaposition of terranes at 3.69 Ga (Nutman & Friend, 2009). Af-

Table 4. A summary of the directions used in the failed pseudo-baked contact tests at sites 4A, B and D.

Sample	Distance from dyke (m)	Range (°C)	Dec (°)	Inc (°)	Origin trending?	MAD	dAng
			Site 4A baked				
4A05	0.8	0–300	252	40	✓	6	16
4A06	1.15	413–580	288	-8	✓	18	4
4A07	1.4	100–375	252	33	✓	4	3
			Site 4A unbaked				
4A10	6.4	375–450	316	-24	✓	8	9
4A11	6.8	100–300	187	33	✓	6	2
4A12	9.7	500–580	160	-34	✓	13	9
4A13	13.2	350–450	208	-25	✓	7	2
			Site B baked				
B11	0.2	220–550	159	44	×	8	13
B13	0.7	290–475	171	-29	✓	5	1
B14	2.2	310–475	321	41	✓	7	0
B29	3	310–475	174	80	✓	7	2
B15	4	220–475	165	-34	✓	9	1
B30	4.9	100–450	197	-57	✓	5	3
B16	6.6	290–475	218	-38	×	6	6
B18	8.1	300–475	148	-61	✓	7	1
B33	10.1	290–450	87	3	✓	10	3
B20	12	220–340	78	29	✓	14	13
B21	12.5	300–475	64	34	✓	9	7
B22	14.4	220–375	309	28	✓	5	3
B23	22.2	300–475	358	46	✓	13	4
			Site B unbaked				
B24	23.3	300–475	61	-43	✓	20	7
B25	24.4	290–475	96	-56	✓	7	3
B26	24.5	150–320	72	-53	×	20	23
B27	25.9	310–450	260	-23	✓	36	13
B28	26	100–475	136	-48	✓	6	3
			Site D baked				
D10	0.7	100–475	241	33	✓	12	2
D09	4.4	220–500	219	4	✓	13	3
D08	5.1	100–500	249	23	✓	10	6
D29	5.3	330–530	232	-18	✓	13	2
D07	5.9	350–500	72	-11	✓	12	7
D06	6.7	220–475	62	24	✓	10	5
D05	10	340–500	246	-12	✓	7	1
D04	10.7	310–500	222	26	✓	17	3
			Site D unbaked				
D26	11	150–530	51	33	×	9	10
D03	11.2	0–500	34	7	✓	7	2
D02	12.1	100–500	348	72	✓	20	8
D24	17.7	150–530	313	5	✓	5	2
D23	20.4	150–530	340	51	✓	7	4

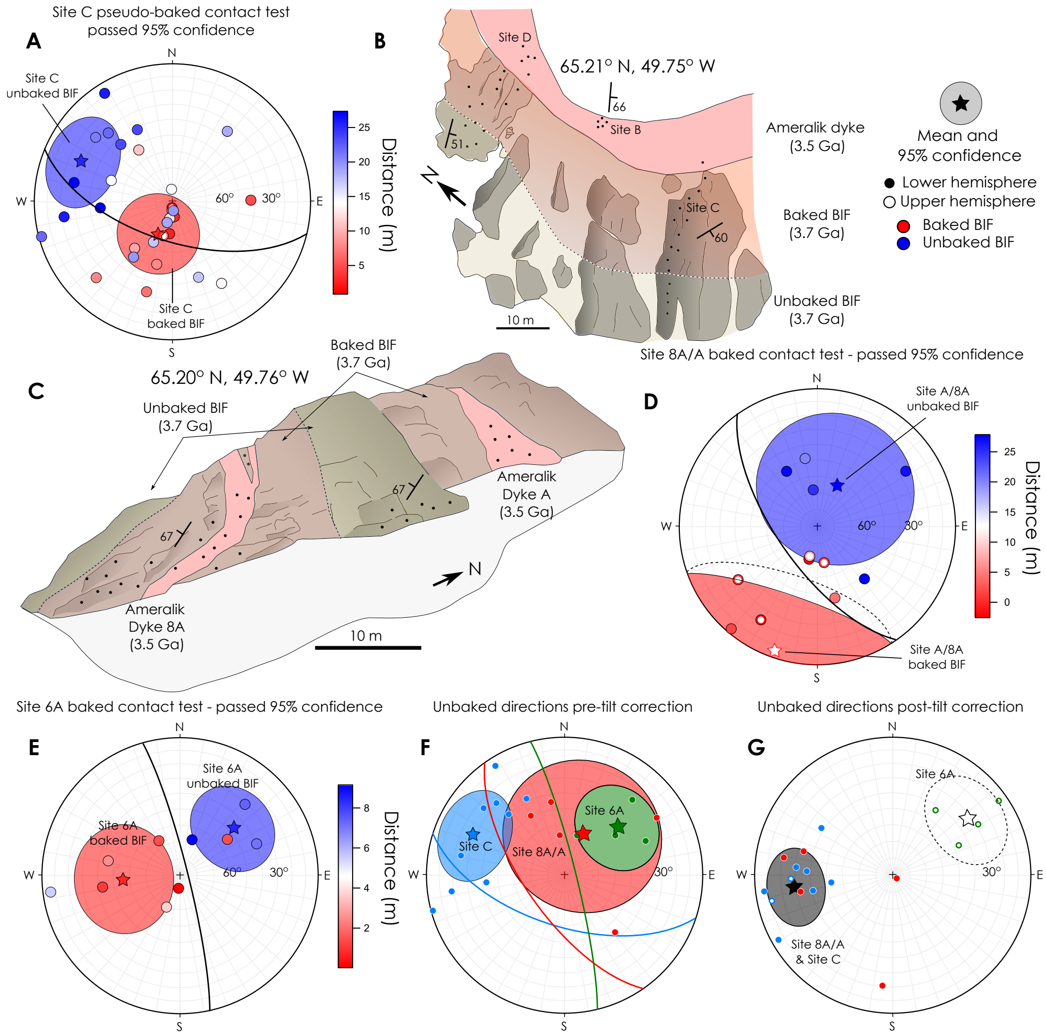

Figure 8. Passed pseudo-baked contact tests in geographic coordinates and unbaked paleodirections in tilt-corrected coordinates. (A) Equal area, lower hemisphere stereoplots showing high temperature (HT) and high coercivity (HC) components recovered for the BIF recovered from Site C. The mean baked BIF direction and unbaked BIF directions are shown by the red and blue stars, respectively. Each recovered paleodirection in the BIF is coloured based on its distance from the dyke contact. (B) An aerial sketch of field sites B, C and D in Zone A. The dyke is shown in red, the baked BIF in orange and unbaked BIF in yellow. (C) An outcrop sketch of site 8A/A. The dykes at site 8A/A are shown in red, the baked BIF is shown in orange and the unbaked BIF in yellow. (D) HT component directions recovered from the baked contact test at sites A and 8A. Each HT direction in the BIF is colour coded with distance from dyke 8A. (E) HT and LT component directions recovered from the baked contact test at site 6A. (F) The HT component directions recovered from the unbaked BIF for each of the passed baked contact tests at site C (blue), site 8A/A (red) and site 6A (green). The directions are shown in geographic coordinates. The basal bedding for each site is shown in the same colour. (G) The HT component directions recovered from the unbaked BIF at each site after tilt correction. The directions from sites C and 8A/A converge (black star) and the direction from site 6A is antipodal (white star). These directions pass a reversal test.

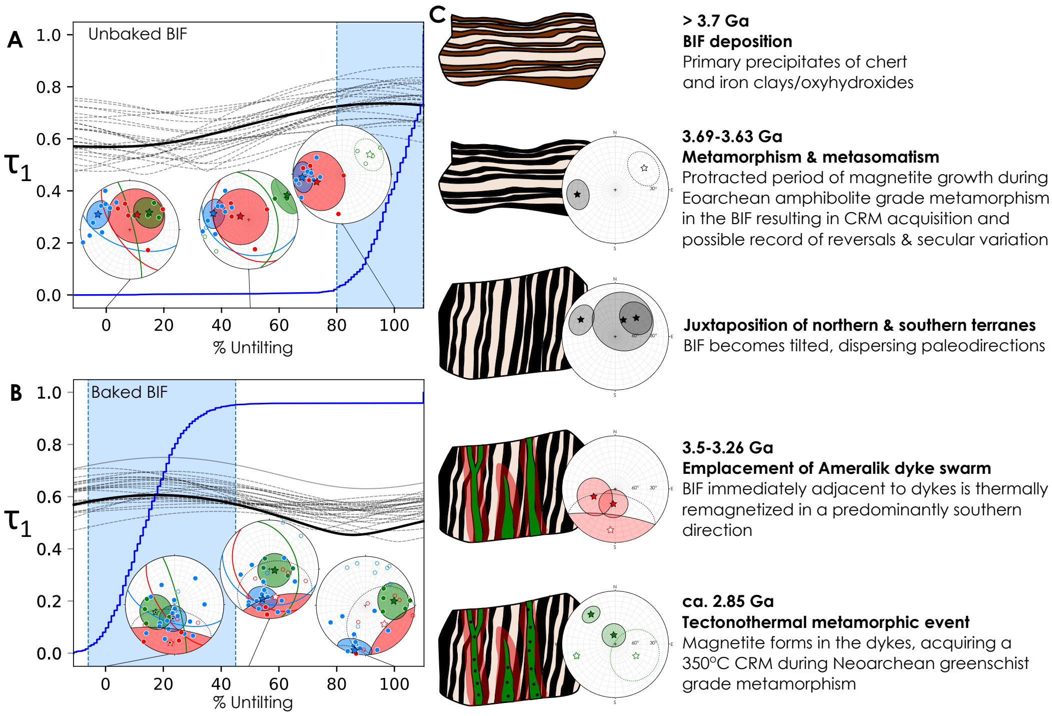

Figure 9. A fold test and the tilting history of the BIF in the ISB. **A** The principal eigenvalue, τ_1, calculated for all the unbaked BIF directions during various degrees of untilting ranging from -10–100%. The maximum value of τ_1 is shaded in blue. The directions for sites 6A, 8A/A and C are shown in green, red and blue, respectively on equal area stereonet projections for 0%, 50% and 100% untilting. **B** As for **A**, for baked BIF. The maximum value of τ_1 was recovered at 20% tilting, suggesting Ameralik and thermal remagnetization of the baked BIF was pre- or syn-tilting. **C** A cartoon schematic showing how the recovered paleomagnetic directions can be interpreted in terms of the geological history of the ISB.

ter untilting, the unbaked paleodirections converge into two antipodal groups, with one direction defined by sites 8A/A and C and the antipodal direction defined by site 6A.

3.5 Reversal Test

We carried out two types of reversal test to determine whether the two antipodal directions recovered after untilting the unbaked BIF directions from sites 6A, 8A/A and C represent a magnetic field reversal. We assume that none of our sites have been overturned, although we were unable to identify any convincing way-up indicators in the field to confirm this. We compared fourteen directions sampled from the fisherian distribution recovered from sites 8A/A and C with four antipodal directions sampled from the fisherian distribution recovered from site 6A. The direction defined by site 6A was rotated 180° to have the same polarity as the direction defined by sites 8A/A and C. The recovered x, y and z directional components of each mean direction were then plotted as cumulative distributions (Figure 10A–C). Bounds that encompass 95% of the data were shown to overlap for all three directional components indicating a passed reversal test (Tauxe et al., 1991).

We also compared the two directions by calculating Watson's V_W statistic for each recovered Fisher distribution of sites 8A/A and C ($N = 14, \kappa = 5$) and 6A flipped to

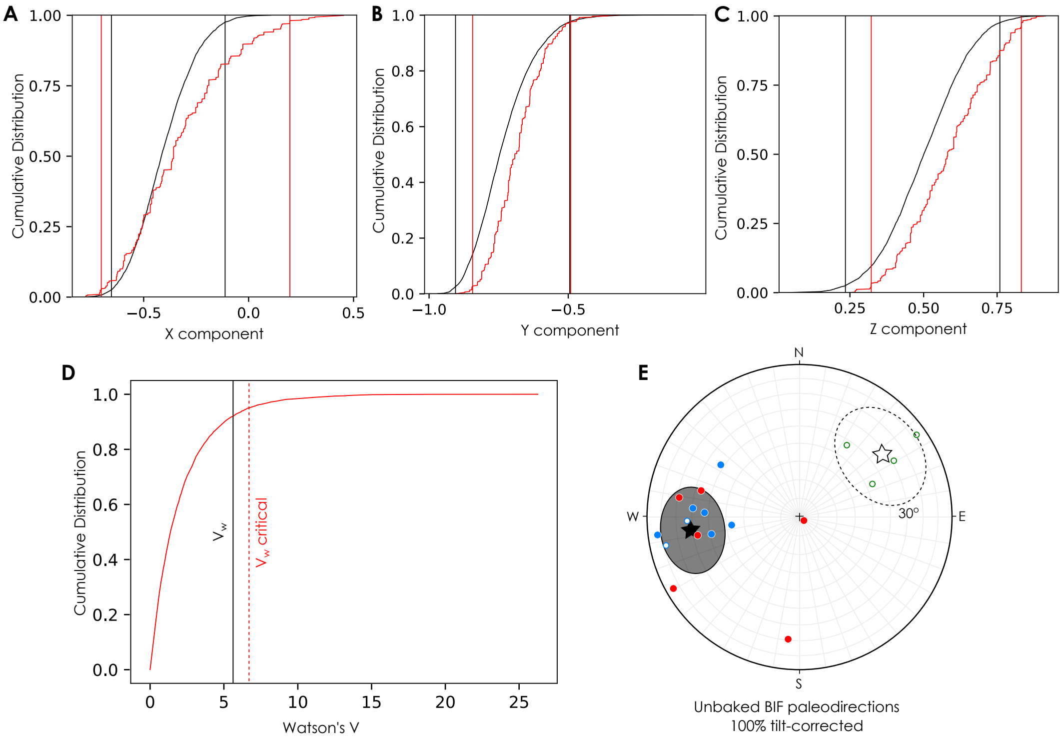

Figure 10. A reversal test for unbaked BIF directions recovered from sites 8A/A, 6A and C. Plots **A**, **B** and **C** show the distribution of x, y and z directional components, respectively. The 95% confidence intervals for each direction overlap for all three components, indicating a passed reversal test. **D** Watson's V_W statistic was calculated and demonstrates that if both directions are rotated to the same polarity, they are indistinguishable to greater than 95% confidence. **E** shows an equal area, lower hemisphere stereonet projection of the recovered paleodirections in red, blue and green for sites 8A/A, C and 6A, respectively.

its antipode ($N = 4, \kappa = 11$), and the critical value of V_W for each by randomly sampling each Fisher distribution 1000 times. The calculated value of V_W falls below the 5th percentile of the cumulative distribution of simulated V_W values, demonstrating that the two directions are indistinguishable with 95% confidence (Figure 10D).

3.6 Pseudo-Thellier paleointensity estimates

Three specimens (A05c, A07c and C02b) from sites 8A/A and C that passed the pseudo-baked contact test, fold test and reversal test were used for Pseudo-Thellier experiments (Paterson et al. (2016); Figure 11). These specimens were also chosen because they are close to the locality where the magnetite in the BIF was U-Pb dated (Frei et al., 1999; Frei & Polat, 2007). Specimens were AF demagnetized up to 145 mT to firstly remove the NRM. A 50 μT ARM was then imparted and again the specimens were demagnetized up to 145 mT. Finally, the samples were given a 40 mT IRM which was also demagnetized up to 145 mT. AF demagnetization of the NRM revealed a HC component which was origin-trending and stable to $>$ 130 mT. The NRM demagnetization was compared to the AF demagnetization of a 50 μT anhysteretic remanent magnetization (ARM). A preliminary paleointensity estimate of 15.1 $\pm$ 1.2 μT (uncertainty is two standard deviations), assuming the NRM represents a TRM, was recovered from all three specimens (Figure 12). One specimen was also corrected for remanence anisotropy (Selkin

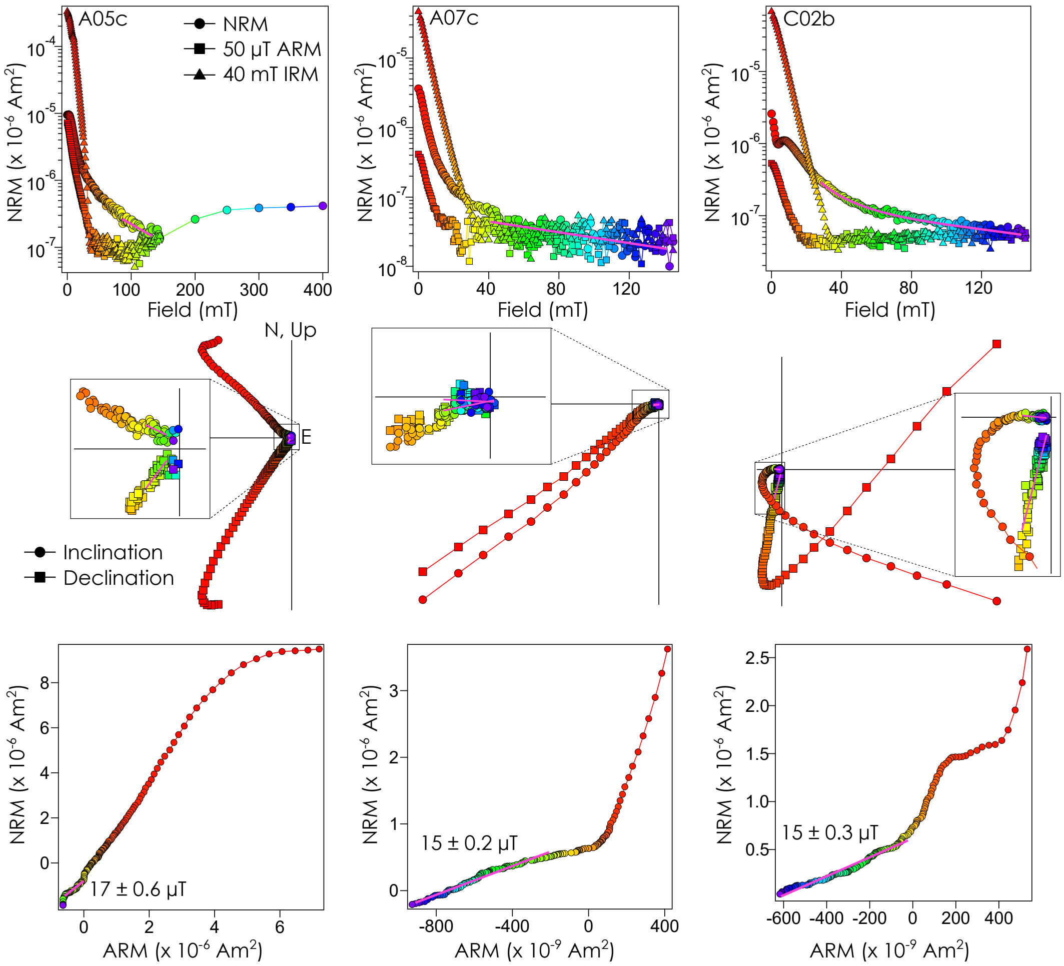

Figure 11. The top panel shows AF demagnetization of an NRM (circles), 50 μT ARM (squares) and 40 mT IRM (triangles) for BIF specimens A05c, A07c, C02b. The middle panel shows zijderveld diagrams for AF demagnetization of the NRMs and HC, origin-trending components are shown by pink lines on the inset panels. On the lowermost panel, NRM vs 50 μT ARM plots are shown. These were used to calculate Pseudo-Thellier paleointensities. The pink line shows origin-trending, HC component over which the paleointensity estimates were calculated.

et al., 2000) which slightly increased the recovered paleointensity to 16.7 $\pm$ 0.7 μT. Since the magnetite in our samples acquired a CRM, these results are taken as evidence for the presence of a field but should not be considered an accurate representation of its strength. CRM acquisition is known to be less efficient than TRM acquisition, but calibrating between the two remains challenging.

Paleointensity estimates were acquired by comparing the vector-subtracted NRM demagnetization to the ARM demagnetization. Three distinctive gradients were observed for specimens A05c and A07c and four for C02b. A paleointensity was calculated for each linear part of the curve between the change in slope. The recovered values vary substantially for the low and medium coercivity components (Table S3). The high coercivity components, which were also origin-trending components for the NRM (Figure 11) return similar paleointensity estimates of 17 ± 1.2 μT, 15 ± 0.4 μT and 15 ± 0.6 μT, respectively (uncertainties are two standard deviations).

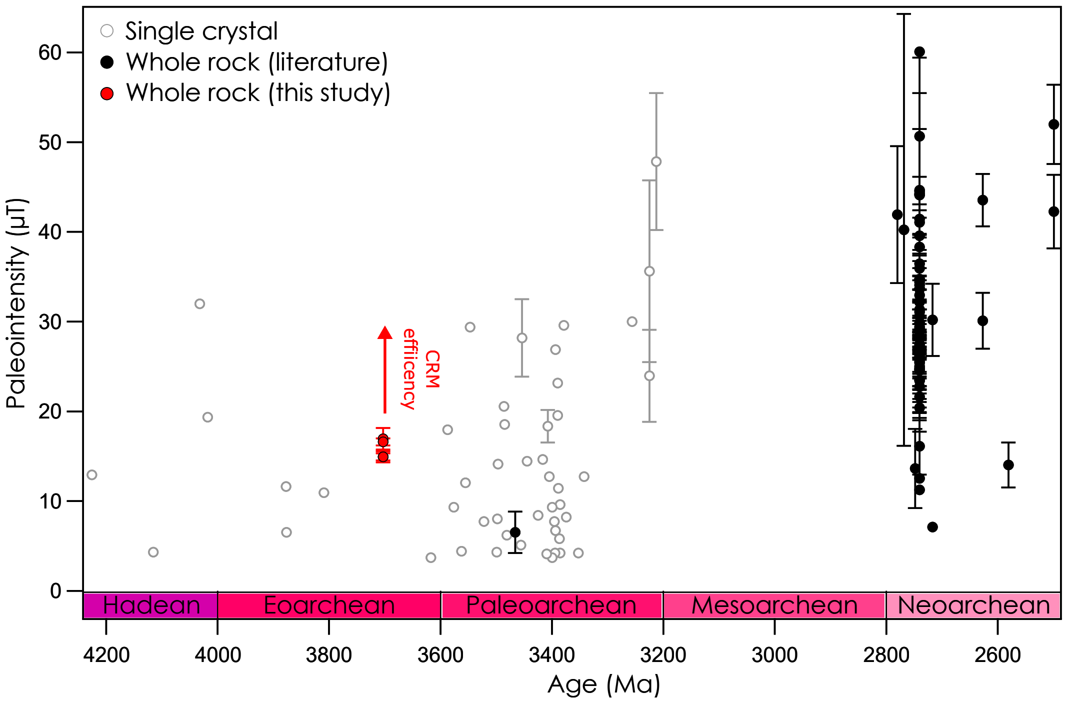

Figure 12. A summary of previous paleointensity studies throughout the Archean and Hadean compiled by Bono et al. (2021). Solid circles represent whole rock studies (Herrero-Bervera et al., 2016; Muxworthy et al., 2013; Biggin et al., 2009; Morimoto et al., 1997; Selkin et al., 2008; Selkin & Tauxe, 2000; Yoshihara & Hamano, 2000; Miki et al., 2009; Shcherbakova et al., 2017) while open circles represent single crystal studies (Tarduno et al., 2015, 2010, 2007). The paleointensities for the three BIF specimens measured here are shown in red. The uncertainty is similar to the size of the circle for the new measurements presented here. The inefficiency of CRM remanence acquisition suggests these intensities likely represent a lower estimate for the Eoarchean geomagnetic field strength (shown by the upward pointing red arrow).

4 Discussion

4.1 The age of dykes and implications for passed pseudo-baked contact tests

We have assumed that the dykes sampled in this study are part of the Ameralik dyke swarm, following the interpretation of Nutman and Friend (2009). However, three sets of Archean dykes are discussed in the literature for this region; the Ameralik, Tarssartôq and Inaluk dykes. The Tarssartôq dykes are thought to be part of the Ameralik dyke swarm (Nutman et al., 2004), with both having basaltic compositions and common inclusion of plagioclase megacrysts. The different nomenclature for these two suites of dykes was adopted to account for the differing extent of deformation, with the Tarssartôq dykes being better preserved (Nutman, 1986). However, a genetic link between the two has never been firmly established (White et al., 2000). The Tarssartôq dykes have an intrusion age of ca. 3550 Ma ago and a U-Pb baddelyite age of 3490 ± 2 Ma (Crowley et al., 2000).

The Inaluk dykes identified in the area are noritic in composition (Nilsson et al., 2010; Nutman, 1986), up to 4 m in diameter and generally folded (White et al., 2000). Their small size and sparse occurrence suggest it is unlikely that these are the dykes we sampled in this study. Nonetheless, they have been dated and have returned ages of 3512 ± 6 Ma, 3659 ± 2 Ma, 3658 ± 1 Ma and 3661 ± 7 Ma (Nutman et al., 2004; Crowley et al., 2000; Crowley, 2003; Friend & Nutman, 2005). Regardless of which type of dykes we sampled in the area, all of them have an age $>$ 3.26 Ga, the younger limit on the emplacement age of the Ameralik dykes. Our passed pseudo-baked contact tests therefore suggest that the magnetization in the unbaked BIF was acquired prior to 3.26 Ga.

4.2 The tectonic history of the ISB and implications for the fold and reversal tests

The ISB has undergone several tectonic events resulting in shearing, tilting and folding. The first major event was the development of a juvenile arc between 3720–3690 Ma ago (Nutman & Friend, 2009; Nutman et al., 2009). The BIF forms part of the central tectonic domain described by Appel et al. (1998) and experienced tight, isoclinal folding prior to its juxtaposition against the rest of the 3.7 Ga northern terrane. The 3.7 Ga northern terrane and 3.8 Ga southern terrane collided 3690–3660 Ma, and subsequently both terranes were sheared by a common event between 3650–3600 Ma (Nutman & Friend, 2009). Arai et al. (2015) also suggest exhumation and faulting of cold, brittle Eoarchean crust following the juxtaposition of the two terranes, although the exact timing of the event is poorly constrained.

A subsequent Noarchean tectonic event occurred ca. 2.85 Ga ago, where the entire northern Isukasia terrane collided with the southern Kapisilik terrane (Nutman, Bennett, Friend, Yi, & Lee, 2015). Large mylonite zones developed $>$ 20 km south of the ISB and are associated with metamorphism 2.69 Ga that metamorphosed some of the Ameralik dykes to epidote-amphibolite grade. The influence of this southern shear zone is minimal in the northern part of the ISB, and is unlikely to have resulted in any major structural deformation. Given that the baked BIF fails the fold test while the unbaked BIF passes, this suggests that folding occurred prior to the emplacement of the dykes $>$ 3.26 Ga, most likely during the tectonic and shearing events 3.69–3.60 Ga. This suggests the remanence in the unbaked BIF was acquired before this time.

Our reversal test is based on the assumption that the BIF at sites 8A/A, 6A and C have not been overturned. We were unable to identify any reliable younging direction indicators in the field, and given the tight isoclinal folding within the BIF we cannot rule out the possibility of overturning. If site 6A is overturned, this would result in the apparent reversed polarity observed at this site. This possibility does not influence the outcome of our fold test which is based on the clustering of directions regardless of polarity (Tauxe et al., 1991). However, we acknowledge that given the complex deformation of the ISB, our reversal test is ambiguous.

4.3 Using paleomagnetic field tests and field observations to reinterpret the tectonothermal history of the northernmost part of the ISB

The metamorphic history of the ISB is complex, and the timing and grade of each metamorphic event remain debated. Part of the difficulty in recovering the tectonothermal history of the area is that the observed metamorphic grades are spatially heterogeneous, and therefore each observation needs to be carefully considered in terms of its geographic location. We have compiled the location of each relevant observation for the three metamorphic events discussed here in Figure 1 and Table 1. One particular discrepancy that is significant for the interpretation of our paleomagnetic data is the differing interpretations regarding the grade of Eoarchean metamorphism in the northernmost part of the field area. Arai et al. (2015) and Komiya et al. (2002) argue that this area of the belt experienced greenschist grade metamorphism ca. 3.71 Ga during exhumation following the collision of the 3.8 Ga southern terrane with the 3.7 Ga northern terrane. However, there are several lines of evidence suggesting this event was amphibolite grade (Table 1) and no evidence for subsequent retrogressive metamorphism (Arai et al., 2015). The magnetite carrying remanence in the BIFs grew during this early metamorphic event, and since HT components demagnetize up to 550°C (Figure 6) we argue this is most consistent with an amphibolite-grade metamorphic event.

The discrepancy between the metamorphic grade interpretations of Arai et al. (2015), Komiya et al. (2002) and other authors (Rollinson, 2003; Nutman et al., 2009; Frei et al., 1999; Dymek & Klein, 1988) can be resolved by considering the difference in their interpretations of the mafic units in the area. The former authors interpret the northernmost part of the ISB as a series of repeatedly faulted pillow basalts and BIF that are stratigraphically conformable. However, Nutman and Friend (2009) interpret the mafic units in this area as Ameralik dykes, and we agree from our own field observations that the relationship between the mafics and BIF is intrusive. All studies (including this one) agree upon the interpretation of the large mafic units in the south as pillow basalts, which are well-preserved and still exhibit clear pillow structures with glassy rims. Therefore, the apparent increase in metamorphic grade from north to south as interpreted by Arai et al. (2015) and Komiya et al. (2002) reflects the Neoarchean greenschist grade metamorphism of the Ameralik dykes in the north, and the pervasive Eoarchean amphibolite grade metamorphism of the pillow basalts in the south of the area.

The Neoarchean metamorphic event is thought to increase in grade from north to south within the larger Isukasia region (Nutman, Bennett, Friend, Yi, & Lee, 2015). In the region where we carried out pseudo-baked contact tests, the metamorphic grade associated with this Neoarchean event has not been directly constrained in detail, although there are several lines of evidence that suggest a lower greenschist grade event with a maximum temperature of 350°C. Neither apatite nor magnetite Pb-Pb ages in the BIF in this area were perturbed during this event, suggesting the peak temperatures were well below the blocking temperatures of both systems (Nishizawa et al., 2005; Frei et al., 1999; Frei & Polat, 2007). The mineral assemblages in the Ameralik dykes are also consistent with greenschist facies conditions (Arai et al., 2015; Komiya et al., 2004). In addition, we find that for all of our pseudo-baked contact tests, the magnetization in the Ameralik dykes is entirely unblocked by ~ 350°C (Figure S15). The subsequent Proterozoic metamorphic event ca. 1.5 Ga did not cause a sufficient thermal perturbation in the northernmost part of the area to influence the recovered Pb-Pb magnetite ages in the BIF (Frei et al., 1999). The observed Neoarchean metamorphic assemblages were also unaffected (Arai et al., 2015), and the 2.2 Ga norite dyke was not metamorphosed and retains its igneous mineralogy (Nutman et al., 2022), although some hydrothermal alteration is observed, which may also account for the perturbation of the Pb-Pb apatite ages in the BIF (Nishizawa et al., 2005).

Our paleomagnetic observations are consistent with a single major amphibolite-grade metamorphic event at 3.69 Ga which resulted in the formation of magnetite, and the corresponding magnetization recovered from the BIFs. We found that remanence was unblocked in the lab at $\sim 550°C$, consistent with an amphibolite grade event (Figure 2B). The Ameralik dykes were emplaced after this Eoarchean metamorphic event, and prior to lower greenschist metamorphism experienced during the Neoarchean ca. 2.85 Ga. The dykes acquired their magnetization during metamorphism, acquiring a low temperature CRM which was unblocked in the lab at 350°C (Figure S15). The subsequent Proterozoic thermal event had a negligible thermal influence, suggesting it reached lower temperatures than the Neoarchean event, consistent with the observed LT overprints that were removed by 100–150°C (Figure 6). We show that neither the Neoarchean nor Proterozoic event could have entirely overprinted the remanence acquired during Eoarchean metamorphism, even if these events lasted for > 0.1 Ga (Figure 2B; Pullaiah et al. (1975)).

4.4 Preservation of an ancient magnetic field record in the Isua Supracrustal Belt

We interpret the magnetization in unbaked BIF as a likely record of paleomagnetic remanence acquired during Eoarchean metamorphism at 3.69 Ga (Dymek & Klein, 1988; Frei et al., 1999). The passed pseudo-baked contact tests suggest the magnetization in the BIF was not overprinted by Neoarchean or Proterozoic metamorphism supporting numerous lines of evidence that neither event exceeded 350°C (Table 1). The convergence of unbaked directions in the BIFs after tilt correction confirms the magnetization was acquired prior to tilting, most likely during the juxtaposition of the 3.7 Ga northern terrane and 3.8 Ga southern terrane at 3.69 Ga (Nutman & Friend, 2009). The consistent southward direction recovered in the baked BIF in geographic coordinates (Figure 8) supports our hypothesis that this magnetization was acquired during Ameralik dyke emplacement 3.26–3.5 Ga, and following tilting.

We have shown that paleomagnetic directions in the BIF can be constrained with sufficient confidence to pass our pseudo-baked contact tests with 95% confidence (Figure 8). We note that anisotropy in BIFs, which is predominantly in the plane of the bands (Schmidt & Clark, 1994), will act to rotate both the unbaked and baked directions into the plane of banding. At each field site studied here, samples were preferentially taken from undeformed bands, and the planar orientation of the bands is approximately constant across each site (as described by our basal bedding measurements). Therefore, any anisotropy correction could be assumed to act to correct all recovered directions in the same way. This will have two effects: first, to focus the recovered directions towards the pole to the plane of banding, reducing the scatter in the observed measurements and second, to increase the angle between recovered baked and unbaked directions in our pseudo-baked contact tests since it will remove the bias that pulls both directions into the plane of the bands, thereby improving the confidence to which they pass.

The high degree of scatter in the recovered directions can be explained by the fact that magnetite grain growth took place over a long time period during metamorphism and therefore remanence was acquired at different times by different populations of grains throughout metamorphism. This may indicate that the scatter in the BIF reflects secular variation of the ancient magnetic field. Our paleodirectional results also suggest the Eoarchean geodynamo may have been reversing. The observed convergence of tilt-corrected results in two antipodal directions (Figure 9) is consistent with a reversing field. Given the uncertainty in the relative timing of remanence acquisition between sites A/8A, C and 6A during metamorphism we cannot constrain a possible reversal rate.

Our results are consistent with previous studies that suggest the Earth's geomagnetic field has been active since the Eoarchean (Tarduno et al., 2015, 2020). Given the slow cooling rates post-metamorphism, it is likely that our paleointensity estimate represents a time-averaged field and may have been further reduced from the 'true' value of the geomagnetic field by reversals, on top of the inefficiency associated with remanence acquisition. Therefore we cannot rule out that the Archean magnetic field was at least as strong as Earth's magnetic field today. This highlights current challenges in accurately recovering the strength and stability of the geomagnetic field over Earth's history, although our results suggest behaviour of the Eoarchean geomagnetic field was similar to that observed today. Recent dynamo models have predicted the magnetic field declined in intensity from the Archean until the Ediacaran (Davies et al., 2022) immediately prior to inner core nucleation. Further constraints on the stability of the Archean field and how this behaviour is manifest in the recovered paleointensity estimates will be required to properly characterize paleointensity trends on billion year timescales.

The paleomagnetic record suggests that Earth has been surrounded by a protective magnetosphere since life originated on its surface. However, our recovered paleointensity of $> 15\ \mu$T is equivalent to a virtual dipole moment of $1.6{\times}10^{22}\text{Am}^2$, suggesting a solar wind standoff distance ~ 5 Earth radii, consistent with previous results (Tarduno et al., 2014). This is approximately half of the standoff distance provided by Earth's magnetosphere today, although we acknowledge our results represent a lower estimate. Recent models have also shown that a weak intrinsic magnetic field can act to increase atmospheric escape via the polar wind, an outflow of ions along open magnetic field lines in the polar regions (Gronoff et al., 2020; Gunell et al., 2018). The degree of atmospheric escape is therefore a trade-off between a larger magnetosphere creating a greater standoff distance that protects the atmosphere from erosion, versus greater connection of open magnetic field lines with the interplanetary magnetic field and increased interaction between the solar wind and atmosphere in the cusp region both of which enhance escape (Vidotto, 2021; Blackman & Tarduno, 2018).

Given the uncertainty in the exact strength of Earth's magnetic field through time and the unknown reversal rate, the delicate balance between magnetic field strength and atmospheric escape could easily be tipped in favour of net atmospheric loss in the presence of a stronger solar wind during the Archean. Further studies should focus on constraining reliable paleointensities in the Archean. Whole-rock, orientable specimens with magnetization ages constrained by U-Pb dating of magnetite should allow time-resolved paleointensity records to be recovered with sufficient time resolution to interrogate the stability and strength of the geomagnetic field during the Archean now the existence of such a field has been confirmed.

5 Conclusions

The ISB contains exceptionally well-preserved crustal rocks from the Eoarchean. In particular, the northern-most part of the northeastern end of the belt has only experienced one high temperature (470–550°C) metamorphic and metasomatic episode during the Eoarchean (Rollinson, 2002, 2003). During this early metamorphic event, magnetite was formed in the BIFs with a Pb-Pb age of 3.69 Ga (Frei et al., 1999). Between 3.26–3.5 Ga the Ameralik dykes were emplaced (Nutman et al., 2004) and thermally reset the BIF immediately adjacent to each intrusion. The dykes were influenced by a subsequent lower greenschist grade metamorphic event in the Neoarchean ca. 2.85 Ga (Arai et al., 2015). A third, low temperature metamorphic event occurred 1.5–1.6 Ga and is observed as perturbations to Pb-Pb, Rb-Sr and Sm-Nd ages (Nishizawa et al., 2005; Polat et al., 2003), but did not have any influence on the observed metamorphic assemblages in the area (Nutman et al., 2022; Arai et al., 2015).

Passed pseudo-baked contacts and fold tests from three sites suggest high-temperature magnetization in the BIF was acquired during Eoarchean amphibolite-grade metamorphism and was not reset by either of the subsequent low grade metamorphic events. The BIFs therefore preserve a primary, high-temperature magnetization from the Eoarchean. Thermal relaxation times for magnetite also indicate that a tectonothermal event with peak temperatures $< 350°C$ would be insufficient to overprint remanences acquired up to 550°C (Pullaiah et al., 1975).

Pseudo-Thellier paleointensity results for the BIF recover an Eoarchean geomagnetic field strength of at least 15.1 ± 1.2 μT. There is significant uncertainty regarding the type of remanence acquired; when magnetite formed during metamorphism it may have acquired a growth CRM, an alteration CRM or a TCRM and therefore paleointensity estimates likely offer only a lower limit on the true intensity. Paleodirectional results suggest the Eoarchean geomagnetic field may have experienced reversals although we were unable to confirm if any of the sampled outcrops of BIF had been overturned. Regardless of its exact strength and stability, our results suggest Earth has sustained an intrinsic magnetic field since at least 3.7 Ga. The role of the geomagnetic field in Earth's habitability is presently ambiguous; a magnetosphere can both shield and enhance atmospheric erosion. The solar wind was substantially stronger during the Archean, and therefore the strength of the geomagnetic field and the frequency of reversals will have had a major influence on the stand-off distance created by the magnetosphere and its effectiveness in shielding Earth from atmospheric loss.

Data Availability

Raw data are available for reviewers at Zenodo: https://doi.org/10.5281/zenodo.8052859. A Jupyter notebook and all relevant data used to run the paleomagnetic field tests in PMagPy is available on GitHub: https://github.com/TinySpaceMagnet/Greenland_Paleomagnetic_Data. All other details of analysis and data interpretation are included in the supplementary materials

Acknowledgments

We thank two anonymous reviewers for their thoughtful comments that have helped to clarify the interpretations presented in this research. CION was funded by the Simons Foundation (grant no. 556352), National Geographic (grant no. EC-50828R-18) and a Lewis and Clark Astrobiology Grant. AE acknowledges support from the MIT EAPS W. O. Crosby and the Johns Hopkins EPS Morton K. Blaustein Postdoctoral Fellowships. SJM, NMK and MJZ were funded by the Collaborative for Research in Origins (CRiO), which was supported by The John Templeton Foundation (principal investigator: Steven Benner/FfAME); the opinions expressed in this publication are those of the authors and do not necessary reflect the views of the John Templeton Foundation. We thank Tim Greenfield for assistance with fieldwork, Jeremy Rushton and Simon Tapster for SEM analysis, Jack Ryan and Richard Harrison for FORC analysis, Matt Beverley-Smith for preparation of polished blocks, Steph Halwa and Rich Palin for assistance with thin section images, and Roger Fishman for drone imagery.

References

Allmendinger, R. W., Cardozo, N. C., & Fisher, D. (2013). Vectors Tensors. In *Structural geology algorithms* (pp. 44–98). Cambridge University Press.

Aoki, S., Kabashima, C., Kato, Y., Hirata, T., & Komiya, T. (2016). Influence of contamination on banded iron formations in the Isua supracrustal belt, West Greenland: Reevaluation of the Eoarchean seawater compositions. *Geoscience Frontiers*, *9*(4), 1049–1072. Retrieved from `http://dx.doi.org/10.1016/`

j.gsf.2016.11.016 doi: 10.1016/j.gsf.2016.11.016
Appel, P. W. U., Fedo, C. M., Moorbath, S., & Myers, J. S. (1998). Recognizable primary volcanic and sedimentary features in a low- strain domain of the highly deformed , oldest known (∼3.7 - 3.8 Gyr) Greenstone Belt, Isua, West Greenland. *Terra Nova*, *10*, 57–62.
Arai, T., Omori, S., Komiya, T., & Maruyama, S. (2015). Intermediate P / T-type regional metamorphism of the Isua Supracrustal Belt , southern west Greenland : The oldest Paci fi c-type orogenic belt ? *Tectonophysics*, *662*, 22–39. Retrieved from http://dx.doi.org/10.1016/j.tecto.2015.05.020 doi: 10.1016/j.tecto.2015.05.020
Badro, J., Siebert, J., & Nimmo, F. (2016). An early geodynamo driven by exsolution of mantle components from Earth's core. *Nature*, *536*, 326–328. Retrieved from http://www.nature.com/doifinder/10.1038/nature18594 doi: 10.1038/nature18594
Biggin, A. J., de Wit, M. J., Langereis, C. G., Zegers, T. E., Voûte, S., Dekkers, M. J., & Drost, K. (2011). Palaeomagnetism of Archaean rocks of the Onverwacht Group, Barberton Greenstone Belt (southern Africa): Evidence for a stable and potentially reversing geomagnetic field at ca. 3.5Ga. *Earth and Planetary Science Letters*, *302*(3-4), 314–328. doi: 10.1016/j.epsl.2010.12.024
Biggin, A. J., Piispa, E. J., Pesonen, L. J., Holme, R., Paterson, G. A., Veikkolainen, T., & Tauxe, L. (2015). Palaeomagnetic field intensity variations suggest Mesoproterozoic inner-core nucleation. *Nature*, *526*(7572), 245–248. Retrieved from http://www.nature.com/doifinder/10.1038/nature15523 doi: 10.1038/nature15523
Biggin, A. J., Strik, G. H., & Langereis, C. G. (2009). The intensity of the geomagnetic field in the late-Archaean: New measurements and an analysis of the updated IAGA palaeointensity database. *Earth, Planets and Space*, *61*(1), 9–22. doi: 10.1186/BF03352881
Blackman, E. G., & Tarduno, J. A. (2018). Mass and energy capture from stellar winds for magnetized and unmagnetized planets: implications for atmospheric erosion and habitability. *Monthly Notices of the Royal Astronomical Society*, *481*(4), 5146–5155. Retrieved from http://arxiv.org/abs/1801.00895 doi: 10.1093/MNRAS/STY2640
Blanc, N. A., Stegman, D. R., & Ziegler, L. B. (2020). Thermal and magnetic evolution of a crystallizing basal magma ocean in Earth's mantle. *Earth and Planetary Science Letters*, *534*, 116085. Retrieved from https://doi.org/10.1016/j.epsl.2020.116085 doi: 10.1016/j.epsl.2020.116085
Bono, R. K., Paterson, G. A., van der Boon, A., Engbers, Y. A., Grappone, J. M., Handford, B., ... Biggin, A. J. (2021). The PINT database: A definitive compilation of absolute palaeomagnetic intensity determinations since 4 billion years ago. *Geophysical Journal International*, 522–545. doi: 10.1093/gji/ggab490
Bono, R. K., Tarduno, J. A., Nimmo, F., & Cottrell, R. D. (2019). Young inner core inferred from Ediacaran ultra-low geomagnetic field intensity. *Nature Geoscience*, *12*(2), 143–147. Retrieved from http://www.nature.com/articles/s41561-018-0288-0 doi: 10.1038/s41561-018-0288-0
Borlina, C., Weiss, B., Lima, E., Tang, F., Taylor, R., Einsle, J., ... Maloof, A. (2020). Re-evaluating the evidence for a Hadean-Eoarchean dynamo. *Science Advances*, *6*, 1–9.
Buchan, K. (2007). Baked Contact Test. In D. Gubbins & E. Herrero-Bervera (Eds.), *Encyclopedia of geomagnetism and paleomagnetism* (pp. 35–55). Springer, Dordrecht. doi: 10.1007/springerreference_77506
Cardozo, N. C., & Allmendinger, R. W. (2013). Spherical projections with OSXStereonet. *Comput. Geosci.*, *51*, 193–205.
Crowley, J. L. (2003). U-Pb geochronology of 3810-3630 Ma granitoid rocks south

of the Isua greenstone belt, southern West Greenland. *Precambrian Research*, *126*(3-4), 235–257. doi: 10.1016/S0301-9268(03)00097-4

Crowley, J. L., White, R. V., Myers, J. S., & Dunning, G. R. (2000). U-Pb geochronology and geologic significance of the two oldest known mafic dyke swarms on earth : 3659 Ma lnaluk dykes and 3490 Ma Tarssartoq dykes , southern west Greenland. *Atlantic Geology*, *36*(November 2000), 3659.

Davies, C. J., Bono, R. K., Meduri, D. G., Aubert, J., Greenwood, S., & Biggin, A. J. (2022). Dynamo constraints on the long-term evolution of Earth's magnetic field strength. *Geophysical Journal International*, *228*(1), 316–336. doi: 10.1093/gji/ggab342

Dymek, R. F., & Klein, C. (1988). Chemistry , Petrology and Origin of Banded Iron- Formation Lithologies From the 3800 Ma Isua Supracrustal Belt , West Greenland. *Precambrian Research*, *39*(4), 247–302. doi: 10.1016/0301-9268(88)90022-8

Erel, Y., Harlavan, Y., Stein, M., & Blum, J. D. (1997). U-Pb dating of Fe-rich phases using a sequential leaching method. *Geochimica et Cosmochimica Acta*, *61*(8), 1697–1703. doi: 10.1016/S0016-7037(97)00028-8

Fedo, C. M. (2000). Setting and origin for problematic rocks from the ¿3.7 Ga Isua Greenstone Belt, southern west Greenland: Earth's oldest coarse clastic sediments. *Precambrian Research*, *101*(1), 69–78. doi: 10.1016/S0301-9268(99)00100-X

Fedo, C. M., Myers, J. S., & Appel, P. W. U. (2001). Depositional setting and paleogeographic implications of earth's oldest supracrustal rocks, the ¿3.7 Ga Isua greenstone belt, West Greenland. *Sedimentary Geology*, *141-142*, 61–77. doi: 10.1016/S0037-0738(01)00068-9

Frei, R., Bridgwater, D., Rosing, M., & Stecher, O. (1999). Controversial Pb-Pb and Sm-Nd isotope results in the early Archean Isua (West Greenland) oxide iron formation: Preservation of primary signatures versus secondary disturbances. *Geochimica et Cosmochimica Acta*, *63*(3-4), 473–488. doi: 10.1016/S0016-7037(98)00290-7

Frei, R., & Polat, A. (2007). Source heterogeneity for the major components of 3.7 Ga Banded Iron Formations (Isua Greenstone Belt, Western Greenland): Tracing the nature of interacting water masses in BIF formation. *Earth and Planetary Science Letters*, *253*(1-2), 266–281. doi: 10.1016/j.epsl.2006.10.033

Friend, C. R. L., & Nutman, A. P. (2005). Complex 3670–3500 Ma Orogenic Episodes Superimposed on Juvenile Crust Accreted between 3850 and 3690 Ma, Itsaq Gneiss Complex, Southern West Greenland. *The Journal of Geology*, *113*(4), 375–397. doi: 10.1086/430239

Gattacceca, J., & Rochette, P. (2004). Toward a robust normalized magnetic paleointensity method applied to meteorites. *Earth and Planetary Science Letters*, *227*(3-4), 377–393. doi: 10.1016/j.epsl.2004.09.013

Gelcich, S., Davis, D. W., & Spooner, E. T. (2005). Testing the apatite-magnetite geochronometer: U-Pb and 40Ar/ 39Ar geochronology of plutonic rocks, massive magnetite-apatite tabular bodies, and IOCG mineralization in Northern Chile. *Geochimica et Cosmochimica Acta*, *69*(13), 3367–3384. doi: 10.1016/j.gca.2004.12.020

Graham, J. W. (1949). The stability and significance of magnetism in sedimentary rocks. *Journal of Geophysical Research*, *54*(2), 131–167.

Gronoff, G., Arras, P., Baraka, S., Bell, J. M., Cessateur, G., Cohen, O., . . . Moore, W. B. (2020). Atmospheric Escape Processes and Planetary Atmospheric Evolution. *Journal of Geophysical Research: Space Physics*, *125*(8), 1–77. doi: 10.1029/2019JA027639

Gruau, G., Rosing, M., Bridgwater, D., & Gill, R. C. (1996). Resetting of Sm-Nd systematics during metamorphism of ¿ 3.7-Ga rocks: implications for isotopic models of early Earth differentiation. *Chemical Geology*, *133*(1-4), 225–240.

doi: 10.1016/S0009-2541(96)00092-7

Gunell, H., Maggiolo, R., Nilsson, H., Stenberg Wieser, G., Slapak, R., Lindkvist, J., . . . De Keyser, J. (2018). Why an intrinsic magnetic field does not protect a planet against atmospheric escape. *Astronomy and Astrophysics*, *614*, 1–8. doi: 10.1051/0004-6361/201832934

Halevy, I., Feldman, Y., Popovitz-Biro, R., Schuster, E. M., & Alesker, M. (2017). A key role for green rust in the Precambrian oceans and the genesis of iron formations. *Nature Geoscience*, *10*(2), 135–139. doi: 10.1038/ngeo2878

Halgedahl, S. L., & Jarrard, R. D. (1995). Low-temperature behavior of single-domain through multidomain magnetite. *Earth and Planetary Science Letters*, *130*(1-4), 127–139. doi: 10.1016/0012-821X(94)00260-6

Harrison, R. J., & Feinberg, J. M. (2008). FORCinel: An improved algorithm for calculating first-order reversal curve distributions using locally weighted regression smoothing. *Geochemistry, Geophysics, Geosystems*, *9*(5). doi: 10.1029/2008GC001987

Herrero-Bervera, E., Krasa, D., & Van Kranendonk, M. J. (2016). A whole rock absolute paleointensity determination of dacites from the Duffer Formation (ca. 3.467 Ga) of the Pilbara Craton, Australia: An impossible task? *Physics of the Earth and Planetary Interiors*, *258*, 51–62. Retrieved from `http://dx.doi.org/10.1016/j.pepi.2016.07.001` doi: 10.1016/j.pepi.2016.07.001

Hirose, K., Morard, G., Sinmyo, R., Umemoto, K., Hernlund, J. W., & Labrosse, S. (2016). SiO2 crystallization and compositional evolution of the Earth's core. *Nature*, 2–12. doi: 10.1038/nature21367

Hodych, J. P. (1982). Magnetostrictive control of coercive force in multidomain magnetite. *Nature*, *298*(5874), 542–544. doi: 10.1038/298542a0

Jaeger, J. C. (1964). Thermal Effects of Intrusions. *Reviews of Geophysics*, *2*(3).

Johnson, J. E., Muhling, J. R., Cosmidis, J., Rasmussen, B., & Templeton, A. S. (2018). Low-Fe(III) Greenalite Was a Primary Mineral From Neoarchean Oceans. *Geophysical Research Letters*, *45*(7), 3182–3192. doi: 10.1002/2017GL076311

Kirschvink, J. L. (1980). The least-squares line and plane and the analysis of palaeomagnetic data. *Geophys. J. R. Astr. Soc.*, *62*, 699–718.

Kobayashi, K. (1959). Chemical Remanent Magnetization of Ferromagnetic Minerals and its Application to Rock Magnetism. *Journal of geomagnetism and geoelectricity*, *10*(3), 99–117. doi: 10.5636/jgg.10.99

Komiya, T., Hayashi, M., Maruyama, S., & Yurimoto, H. (2002). Intermediate-P/T type Archean metamorphism of the Isua supracrustal belt: Implications for secular change of geothermal gradients at subduction zones and for Archean plate tectonics. *American Journal of Science*, *302*(9), 806–826. doi: 10.2475/ajs.302.9.806

Komiya, T., Maruyama, S., Hirata, T., Yurimoto, H., & Nohda, S. (2004). Geochemistry of the oldest MORB and OIB in the Isua Supracrustal Belt, southern West Greenland: Implications for the composition and temperature of early Archean upper mantle. *Island Arc*, *13*(1), 47–72. doi: 10.1111/j.1440-1738.2003.00416.x

Konhauser, K. O., Planavsky, N. J., Hardisty, D. S., Robbins, L. J., Warchola, T. J., Haugaard, R., . . . Johnson, C. M. (2017). Iron formations: A global record of Neoarchaean to Palaeoproterozoic environmental history. *Earth-Science Reviews*, *172*(June), 140–177. Retrieved from `https://doi.org/10.1016/j.earscirev.2017.06.012` doi: 10.1016/j.earscirev.2017.06.012

Konôpková, Z., McWilliams, R. S., Gómez-Pérez, N., & Goncharov, A. F. (2016). Direct measurement of thermal conductivity in solid iron at planetary core conditions. *Nature*, *534*(7605), 99–101. Retrieved from `http://www.nature.com/doifinder/10.1038/nature18009` doi: 10.1038/nature18009

Landeau, M., Fournier, A., Nataf, H.-C., Cébron, D., & Schaeffer, N. (2022). Sustaining Earth's magnetic dynamo. *Nature Reviews Earth Environment*, *0123456789*. doi: 10.1038/s43017-022-00264-1

Lowrie, W., & Fuller, M. (1971). On the alternating field demagnetization characteristics of multidomain thermoremanent magnetization in magnetite. *Journal of Geophysical Research*, *76*(26), 6339–6349. doi: 10.1029/jb076i026p06339

Lundin, R., Lammer, H., & Ribas, I. (2007). Planetary magnetic fields and solar forcing: Implications for atmospheric evolution. *Space Science Reviews*, *129*(1-3), 245–278. doi: 10.1007/s11214-007-9176-4

Maxbauer, D. P., Feinberg, J. M., & Fox, D. L. (2016). MAX UnMix: A web application for unmixing magnetic coercivity distributions. *Computers and Geosciences*, *95*, 140–145. Retrieved from `http://dx.doi.org/10.1016/j.cageo.2016.07.009` doi: 10.1016/j.cageo.2016.07.009

Miki, M., Taniguchi, A., Yokoyama, M., Gouzu, C., Hyodo, H., Uno, K., … Otofuji, Y. I. (2009). Palaeomagnetism and geochronology of the proterozoic dolerite dyke from southwest greenland: Indication of low palaeointensity. *Geophysical Journal International*, *179*(1), 18–34. doi: 10.1111/j.1365-246X.2009.04258.x

Moorbath, S., O'Nions, R. K., & Pankhurst, R. J. (1973). Early Archean Age for the Isua Iron Formation, West Greenland. *Nature*, *245*, 138–139. Retrieved from `https://engineering.purdue.edu/$\sim$yep/Papers/NatureNanotechnologyMoS2NCFET2017plussupplement.pdf` doi: 10.1038/s41565-017-0010-1

Morimoto, C., Otofuji, Y. I., Miki, M., Tanaka, H., & Itaya, T. (1997). Preliminary palaeomagnetic results of an Archaean dolerite dyke of west Greenland: Geomagnetic field intensity at 2.8 Ga. *Geophysical Journal International*, *128*(3), 585–593. doi: 10.1111/j.1365-246X.1997.tb05320.x

Muxworthy, a. R., Evans, M. E., Scourfield, S. J., & King, J. G. (2013, jul). Paleointensity results from the late-Archaean Modipe Gabbro of Botswana. *Geochemistry, Geophysics, Geosystems*, *14*(7), 2198–2205. Retrieved from `http://doi.wiley.com/10.1002/ggge.20142` doi: 10.1002/ggge.20142

Nilsson, M. K., Söderlund, U., Ernst, R. E., Hamilton, M. A., Scherstén, A., & Armitage, P. E. (2010). Precise U-Pb baddeleyite ages of mafic dykes and intrusions in southern West Greenland and implications for a possible reconstruction with the Superior craton. *Precambrian Research*, *183*(3), 399–415. Retrieved from `http://dx.doi.org/10.1016/j.precamres.2010.07.010` doi: 10.1016/j.precamres.2010.07.010

Nishizawa, M., Takahata, N., Terada, K., Komiya, T., Ueno, Y., & Sano, Y. (2005). Rare-earth element, lead, carbon, and nitrogen geochemistry of apatite-bearing metasediments from the similar to 3.8 Ga Isua supracrustal belt, West Greenland. *International Geology Review*, *47*(9), 952–970. doi: 10.2747/0020-6814.47.9.952

Nutman, A. P. (1986). The early Archaean to Proterozoic history of the Isukasia area, southern West Greenland. *Gronlands Geologiske Undersogelse Bulletin*, *154*(22295), 80. doi: 10.34194/bullggu.v154.6696

Nutman, A. P., Allaart, J. A. N. H., & Bridgwater, D. (1984). Stratigraphic and geochemical evidence for the depositional environment of the early Archean Isua Supracrustal Belt, southern west Greenland. *Precambrian Research*, *25*(April 1982), 365–396.

Nutman, A. P., Bennett, V. C., & Friend, C. (2015). The emergence of the Eoarchaean proto-arc: Evolution of a c. 3700 Ma convergent plate boundary at Isua, southern West Greenland. *Geological Society Special Publication*, *389*(1), 113–133. Retrieved from `http://sp.lyellcollection.org/lookup/doi/10.1144/SP389.5` doi: 10.1144/SP389.5

Nutman, A. P., Bennett, V. C., & Friend, C. R. (2017). Seeing through the magnetite: Reassessing Eoarchean atmosphere composition from Isua (Greenland)

3.7 Ga banded iron formations. *Geoscience Frontiers*, *8*(6), 1233–1240. doi: 10.1016/j.gsf.2017.02.008

Nutman, A. P., Bennett, V. C., Friend, C. R., Yi, K., & Lee, S. R. (2015). Mesoarchaean collision of Kapisilik terrane 3070Ma juvenile arc rocks and ¿3600Ma Isukasia terrane continental crust (Greenland). *Precambrian Research*, *258*, 146–160. Retrieved from `http://dx.doi.org/10.1016/j.precamres.2014.12.013` doi: 10.1016/j.precamres.2014.12.013

Nutman, A. P., & Friend, C. R. (2009). New 1:20,000 scale geological maps, synthesis and history of investigation of the Isua supracrustal belt and adjacent orthogneisses, southern West Greenland: A glimpse of Eoarchaean crust formation and orogeny. *Precambrian Research*, *172*(3-4), 189–211. doi: 10.1016/j.precamres.2009.03.017

Nutman, A. P., Friend, C. R., Bennett, V. C., Yi, K., & Van Kranendonk, M. (2022). Review of the Isua supracrustal belt area (Greenland) Eoarchean geology from integrated 1:20,000 scale maps, field observations and laboratory data: Constraints on early geodynamics. *Precambrian Research*, *379*(June), 106785. Retrieved from `https://doi.org/10.1016/j.precamres.2022.106785` doi: 10.1016/j.precamres.2022.106785

Nutman, A. P., Friend, C. R., & Paxton, S. (2009). Detrital zircon sedimentary provenance ages for the Eoarchaean Isua supracrustal belt southern West Greenland: Juxtaposition of an imbricated ca. 3700 Ma juvenile arc against an older complex with 3920-3760 Ma components. *Precambrian Research*, *172*(3-4), 212–233. doi: 10.1016/j.precamres.2009.03.019

Nutman, A. P., Friend, C. R. L., Bennett, V. C., & MCGregor, V. R. (2004). Dating of the Ameralik dyke swarms of the Nuuk district, southern West Greenland: mafic intrusion events starting from c. 3510 Ma. *Journal of the Geological Society*, *161*(3), 421–430. Retrieved from `http://jgs.lyellcollection.org/cgi/doi/10.1144/0016-764903-043` doi: 10.1144/0016-764903-043

Nutman, A. P., Hagiya, H., & Maruyama, S. (1995). SHRIMP U-Pb single zircon geochronology of a Proterozoic mafic dyke, Isukasia, southern West Greenland. *Bulletin of the Geological Society of Denmark*, *42*, 17–2210.

Ohta, K., Kuwayama, Y., Hirose, K., Shimizu, K., & Ohishi, Y. (2016). Experimental determination of the electrical resistivity of iron at Earth's core conditions. *Nature*, *534*(7605), 95–98. Retrieved from `http://www.nature.com/doifinder/10.1038/nature17957` doi: 10.1038/nature17957

O'Rourke, J. G., & Stevenson, D. J. (2016). Powering Earth's dynamo with magnesium precipitation from the core. *Nature*, *529*(7586), 387–389. Retrieved from `http://dx.doi.org/10.1038/nature16495` doi: 10.1038/nature16495

Paterson, G. A., Heslop, D., & Pan, Y. (2016). The pseudo-Thellier palaeointensity method: New calibration and uncertainty estimates. *Geophys.*, *207*(3), 1596–1608. doi: 10.1093/gji/ggw349

Polat, A., Hofmann, A. W., Münker, C., Regelous, M., & Appel, P. W. (2003). Contrasting geochemical patterns in the 3.7-3.8 Ga pillow basalt cores and rims, Isua greenstone belt, Southwest Greenland: Implications for postmagmatic alteration processes. *Geochimica et Cosmochimica Acta*, *67*(3), 441–457. doi: 10.1016/S0016-7037(02)01094-3

Pozzo, M., Davies, C., Gubbins, D., & Alfè, D. (2012, may). Thermal and electrical conductivity of iron at Earth's core conditions. *Nature*, *485*(7398), 355–358. Retrieved from `http://www.ncbi.nlm.nih.gov/pubmed/22495307` doi: 10.1038/nature11031

Pullaiah, G., Irving, E., Buchan, K., & Dunlop, D. (1975). Magnetization changes caused by burial and uplift. *Earth and Planetary Science Letters*, *28*, 133–143. doi: 10.1017/s0252921100050831

Rasmussen, B., & Muhling, J. R. (2018). Making magnetite late again: Evidence for widespread magnetite growth by thermal decomposition of siderite in Hamersley banded iron formations. *Precambrian Research*, *306*(December 2017), 64–93. Retrieved from https://doi.org/10.1016/j.precamres.2017.12.017 doi: 10.1016/j.precamres.2017.12.017

Rollinson, H. (2002). The metamorphic history of the Isua Greenstone Belt, West Greenland. *Geological Society Special Publication*, *199*(1), 329–350. doi: 10.1144/GSL.SP.2002.199.01.16

Rollinson, H. (2003). Metamorphic history suggested by garnet-growth chronologies in the Isua Greenstone Belt, West Greenland. *Precambrian Research*, *126*(3-4), 181–196. doi: 10.1016/S0301-9268(03)00094-9

Schmidt, P. W., & Clark, D. A. (1994). Palaeomagnetism and magnetic anisotropy of proterozoic banded-iron formations and iron ores of the Hamersley Basin Western Australia. *Exploration Geophysics*, *24*(2), 223–226. doi: 10.1071/EG993223

Selkin, P. A., Gee, J. S., Meurer, W. P., & Hemming, S. R. (2008). Paleointensity record from the 2.7 Ga Stillwater Complex, Montana. *Geochemistry, Geophysics, Geosystems*, *9*(12). doi: 10.1029/2008GC001950

Selkin, P. A., Gee, J. S., Tauxe, L., Meurer, W. P., & Newell, A. J. (2000). The effect of remanence anisotropy on paleointensity estimates: A case study from the Archean Stillwater Complex. *Earth and Planetary Science Letters*, *183*(3-4), 403–416. doi: 10.1016/S0012-821X(00)00292-2

Selkin, P. A., & Tauxe, L. (2000). Long-term variations in palaeointensity. *Philosophical Transactions of the Royal Society A: Mathematical, Physical and Engineering Sciences*, *358*(1768), 1065–1088. Retrieved from http://rsta.royalsocietypublishing.org/content/358/1768/1065 doi: 10.1098/rsta.2000.0574

Shcherbakova, V. V., Lubnina, N. V., Shcherbakov, V. P., Zhidkov, G. V., & Tsel'movich, V. A. (2017). Paleointensity determination on Neoarchaean dikes within the Vodlozerskii terrane of the Karelian craton. *Izvestiya, Physics of the Solid Earth*, *53*(5), 714–732. doi: 10.1134/S1069351317050111

Stokking, L. B., & Tauxe, L. (1987). Acquisition of chemical remanent magnetization by synthetic iron oxide. *Nature*, 18–20.

Stokking, L. B., & Tauxe, L. (1990). Properties of chemical remanence in synthetic hematite: Testing theoretical predictions. *Journal of Geophysical Research*, *95*(89), 639–652.

Tang, F., Taylor, R. J. M., Einsle, J. F., Borlina, C. S., Fu, R. R., Weiss, Benjamin P Williams, H., … Bell , Elizabeth A. Harrison, T. Mark Alexander, Ellen Harrison, R. J. (2019). Secondary magnetite in ancient zircon precludes analysis of a Hadean geodynamo. *Proceedings of the National Academy of Sciences*, *116*(2), 407–412. doi: 10.1073/pnas.1811074116

Tarduno, J. A., Blackman, E. G., & Mamajek, E. E. (2014). Detecting the oldest geodynamo and attendant shielding from the solar wind: Implications for habitability. *Physics of the Earth and Planetary Interiors*, *233*, 68–87. Retrieved from http://dx.doi.org/10.1016/j.pepi.2014.05.007 doi: 10.1016/j.pepi.2014.05.007

Tarduno, J. A., Cottrell, R. D., Bono, R. K., Oda, H., Davis, W. J., & Fayek, M. (2020). Paleomagnetism indicates that primary magnetite in zircon records a strong Hadean geodynamo. *Proceedings of the National Academy of Sciences*, 1–10. doi: 10.1073/pnas.1916553117

Tarduno, J. A., Cottrell, R. D., Davis, W. J., Nimmo, F., & Bono, R. K. (2015). Supplementary Material for A Hadean to Paleoarchean geodynamo recorded by single zircon crystals. *Science*, *521*(July). doi: 10.1126/science.aaa9114

Tarduno, J. A., Cottrell, R. D., Watkeys, M. K., & Bauch, D. (2007). Geomagnetic field strength 3.2 billion years ago recorded by single silicate crystals. *Nature*, *446*(7136), 657–660. doi: 10.1038/nature05667

Tarduno, J. A., Cottrell, R. D., Watkeys, M. K., Hofmann, A., Doubrovine, P. V., Mamajek, E. E., ... Usui, Y. (2010). Geodynamo, solar wind, and magnetopause 3.4 to 3.45 billion years ago. *Science*, *327*(5970), 1238–1240. doi: 10.1126/science.1183445

Tauxe, L., Kylstra, N., & Constable, C. (1991). Bootstrap statistics for paleomagnetic data. *Journal of Geophysical Research*, *96*(B7), 11723–11740. doi: 10.1029/91jb00572

Tauxe, L., & Watson, G. S. (1994). The fold test: an eigen analysis approach. *Earth and Planetary Science Letters*, *122*(3-4), 331–341. doi: 10.1016/0012-821X(94)90006-X

Taylor, R. J., Reddy, S. M., Saxey, D. W., Rickard, W. D., Tang, F., Borlina, C. S., ... Harrison, R. J. (2023). Direct age constraints on the magnetism of Jack Hills zircon. *Science advances*, *9*(1), eadd1511. doi: 10.1126/sciadv.add1511

Tosca, N. J., Guggenheim, S., & Pufahl, P. K. (2016). An authigenic origin for Precambrian greenalite: Implications for iron formation and the chemistry of ancient seawater. *Bulletin of the Geological Society of America*, *128*(3-4), 511–530. doi: 10.1130/B31339.1

Vidotto, A. A. (2021). *The evolution of the solar wind* (Vol. 18) (No. 1). Springer International Publishing. Retrieved from `https://doi.org/10.1007/s41116-021-00029-w` doi: 10.1007/s41116-021-00029-w

Wabo, H., Maré, L. P., Beukes, N. J., Kruger, S. J., Humbert, F., & De Kock, M. O. (2018). Mineral transformations during thermal demagnetization of sideritic jasper mesobands in jaspilites of the ∼3.25 Ga Fig Tree Group in the Barberton Greenstone Belt, Kaapvaal craton (South Africa). *South African Journal of Geology*, *121*(2), 131–140. doi: 10.25131/sajg.121.0010

Watson, E. B., Cherniak, D. J., Nichols, C. I. O., & Weiss, B. P. (2023). Pb diffusion in magnetite: dating magnetite crystallization and the timing of remanent magnetization in banded iron formation. *Chemical Geology*.

Watson, G. S. (1965). A test for randomness of directions. *Geophysical Supplements to the Monthly Notices of the Royal Astronomical Society*, *7*(4), 160–161.

Watson, G. S. (1983). Large sample theory of the Langevin distribution. *Journal of Statistical Planning and Inference*, *8*(3), 245–256. doi: 10.1016/0378-3758(83)90043-5

Weiss, B. P., Fu, R. R., Einsle, J. F., Glenn, D. R., Kehayias, P., Bell, E. A., ... Harrison, R. J. (2018). Secondary magnetic inclusions in detrital zircons from the Jack Hills , Western Australia and implications for the origin of the geodynamo microscopy. *Geology*, *46*. doi: 10.1130/G39938.1

Weiss, B. P., Maloof, A. C., Tailby, N., Ramezani, J., Fu, R. R., Hanus, V., ... Coe, R. S. (2015). Pervasive remagnetization of detrital zircon host rocks in the Jack Hills, Western Australia and implications for records of the early geodynamo. *Earth and Planetary Science Letters*, *430*, 115–128. Retrieved from `http://dx.doi.org/10.1016/j.epsl.2015.07.067http://linkinghub.elsevier.com/retrieve/pii/S0012821X15005105` doi: 10.1016/j.epsl.2015.07.067

White, R. V., Crowley, J. L., & Myers, J. S. (2000). Earth ' s oldest well-preserved mafic dyke swarms in the vicinity of the Isua greenstone belt , southern West Greenland. *Episodes*, *72*, 65–72.

Yoshihara, A., & Hamano, Y. (2000). Intensity of the Earth's magnetic field in late Archean obtained from diabase dikes of the Slave Province, Canada. *Physics of the Earth and Planetary Interiors*, *117*(1-4), 295–307. doi: 10.1016/S0031-9201(99)00103-X

Zhang, Y., Hou, M., Liu, G., Zhang, C., Prakapenka, V. B., Greenberg, E., ... Lin, J.-F. F. (2020). Reconciliation of Experiments and Theory on Transport Properties of Iron and the Geodynamo. *Physical Review Letters*, *125*(7), 78501. Retrieved from `https://doi.org/10.1103/PhysRevLett.125.078501` doi: 10.1103/PhysRevLett.125.078501